Atmospheric
Chemistry
and Physics
Discussions

IAP-AACM v1.0： Global to regional evaluation of the atmospheric chemistry model in CAS-ESM

Ying Wei[1,2], Xueshun Chen[1,4], Huansheng Chen[1], Jie Li[1], Zifa Wang[1,2,4], Wenyi Yang[1], Baozhu Ge[1], Huiyun Du[1,2], Jianqi Hao[1,*], Wei Wang[3], Jianjun Li[3], Yele Sun[1], Huili Huang[1]

5

[1] The State Key Laboratory of Atmospheric Boundary Layer Physics and Atmospheric Chemistry, Institute of Atmospheric Physics, Chinese Academy of Sciences, Beijing 100029, China

[2] University of Chinese Academy of Sciences, Beijing 100049, China

10　[3] China National Environmental Monitoring Center, Beijing 100012, China

[4] Center for Excellence in Regional Atmospheric Environment, Institute of Urban Environment, Chinese Academy of Sciences, Xiamen 361021, China

[*] Now at: School of Civil and Environmental Engineering, Georgia Institute of Technology, Atlanta, GA, 30332, USA

15　*Correspondence to*: Zifa Wang (zifawang@mail.iap.ac.cn)

Abstract:

In this study, a full description and comprehensive evaluation of a global-regional nested model, the Aerosol and Atmospheric Chemistry Model of the Institute of Atmospheric Physics (IAP-AACM), is presented for the first time. Not only the global

20　budgets and distribution, but also a comparison of nested simulation over China against multi-datasets are investigated, benefiting from the access of air quality monitoring data in China since 2013 and the Model Inter-Comparison Study for Asia

Atmospheric
Chemistry
and Physics
Discussions

project. The model results and analysis can greatly help reduce uncertainties and understand model diversity in assessing global and regional aerosol effects, especially

25 over East Asia and areas affected by East Asia. The 1-year simulation for 2014 shows that the IAP-AACM is within the range of other models, and well reproduces both spatial distribution and seasonal variation of trace gases and aerosols over major continents and oceans (mostly within the factor of two). The model nicely captures spatial variation for carbon monoxide except an underestimation over the ocean that

30 also shown in other models, which suggests the need for more accurate emission rate of ocean source. For aerosols, the simulation of fine-mode particulate matter ($PM_{2.5}$) matches observation well and it has a better simulating ability on primary aerosols than secondary aerosols. This calls for more investigation on aerosol chemistry. Furthermore, IAP-AACM shows the superiority of global model, compared with

35 regional model, on performing regional transportation for the nested simulation over East Asia. For the city evaluation over China, the model reproduces variation of sulfur dioxide (SO_2), nitrogen dioxide (NO_2) and $PM_{2.5}$ accurately in most cities, with correlation coefficients above 0.5. Compared to the global simulation, the nested simulation exhibits an improved ability to capture the high temporal and spatial

40 variability over China. In particular, the correlation coefficients for $PM_{2.5}$, SO_2 and NO_2 are raised by ~0.25, ~0.15 and ~0.2 respectively in the nested grid. The summary provides constructive information for the application of chemical transport models. In future, we recommend the model's ability to capture high spatial variation of $PM_{2.5}$ is yet to be improved.

Atmospheric
Chemistry
and Physics
Discussions

Open Access

EGU

1. Introduction

Atmospheric composition can affect climate and environment through direct and

indirect effects (Intergovernmental Panel on Climate Change (IPCC), 2001). The

50 composition of the troposphere has changed a lot due to anthropogenic activities over

the past decades (Akimoto, 2003; Tsigaridis et al., 2006). Changes in the

concentration of trace gases such as SO_2 and nitrogen oxides ($NO_x = NO + NO_2$) have

a substantial impact on acid deposition (Mathur et al., 2003), atmospheric oxidation

(Calvert, 1984), and gas-particle transformation processes (Saxena et al., 1987).

55 Formation of aerosol from these precursor gases, together with aerosol from other

sources, have a direct radiative forcing which is estimated to be -0.3 ~ -1.0 W m^{-2},

with a factor of two uncertainty (Luo et al., 1998). By modifying cloud properties, the

aerosols also have important indirect effects. As reported in the Fourth Assessment

Report (AR4) of IPCC (2007), the first indirect radiative forcing of aerosol ranges

60 from -1.8 ~ -0.3 W m^{-2}. This is more accurate than the result presented in IPCC AR3

(Penner et al., 2001) which ranges from -2.0 ~ 0 W m^{-2}, but there is still much

uncertainty. In addition, aerosols have adverse impacts on human health including

respiratory diseases and lung cancer, which has drawn increasing public attention (Li

et al., 2006; Kan and Chen ,2002; Pope et al., 2002). It is necessary to represent the

65 key physical and chemical parameters controlling trace gases and aerosols in order to

quantify these adverse effects and project the influence of aerosols in the future (IPCC, 2007).

Chemical Transport Models (CTMs) are mathematical tools for studying the evolution of chemical constituents in the atmosphere. CTMs have irreplaceable

70   advantages in terms of source and sink assessment of trace gases, historical process reproduction, and future scenario prediction. CTMs, together with observations and laboratory simulations, have become the main methods for atmospheric environmental research (Wang et al., 2008). But there are numerous uncertain factors affecting model results (e.g. meteorology, emissions and model framework and

75   physiochemical schemes). Therefore, model evaluation is essential for model development and scientific analysis. To date, many assessments with a single model using various observation datasets and multi-model inter-comparisons (with or without observations) have provided us with a comprehensive understanding of model performance and uncertainty. e.g., Badia et al. (2017) evaluated the gas-phase

80   chemistry of the Multi-scale Online Nonhydrostatic Atmosphere Chemistry model (NMMB-MONARCH), Mann et al. (2010) evaluated both mass concentration and number concentration of the Global Model of Aerosol Processes (GLOMAP), and Tsigaridis et al. (2014) gave a detail evaluation of organic aerosol in the Aerosol Comparisons between Observations and Models Project (AeroCom). However,

85   evaluation against site observation are mainly for America and Europe while inadequate for EA due to a limited set of data (Søvde et al., 2012; Lee et al., 2015; Kaiser et al. 2018). Besides, observation of China is scarcely included in model

Atmospheric
Chemistry
and Physics
Discussions

evaluation. Spatial distribution of aerosols affects estimation of radiative forcing (Shindell et al., 2013; Giorgi et al., 2003). Thereby, more observation used to test the

90   model results enables us to reduce uncertainties of climate effect prediction over EA.

Along with economic development and urbanization, most megacities in China have been plagued by haze in recent years. There are many reports on observation and simulation studies addressing particulate matter. The model studies mainly focus on the relationship between haze and weather conditions (Zhang et al., 2015; Tie et al.,

95   2015, 2017), pollutant source apportionment (Wang et al., 2013; Wang et al., 2014), and the chemical mechanism of particulate formation (Cheng et al., 2016). Regional models are more often used in local air pollution research due to its precise ability to capture the variation of inputs (e.g. meteorology, underlying surface and emissions) and therefrom the temporal and spatial variation of pollutants. However, the setting of

100   boundary condition limits continuous transportation from upwind and may lead to unrealistic description in the model.

Based on the Global Nested Grid Air Quality Prediction Model System (GNAQPMS) (Chen et al., 2015), we developed IAP-AACM and coupled it into CAS-ESM (the Earth System Model of the Chinese Academy of Science) as the

105   atmosphere chemistry component of the model, using the framework of coupler 7 (CPL7) (Tang et al., 2015；Zhu et al., 2018). As a multi-scale nested aerosol model based on air quality prediction in China, IAP-AACM not only has the capability for global and regional simulations, but also has strengths in localization of the process parameterization (e.g. dust mode and heterogeneous chemistry) (Wang et al., 2000; Li

110   et al., 2018). The development of IAP-AACM allows us to quantify climate effects on

a global scale and elucidate air pollution problems on a regional scale over China.

Here a large number of datasets are used to evaluate the model, including a dataset of

city sites covering China. Continuous year-round observations at city sites can help

study of air pollution and model evaluation in China. As we are currently building a

115   global forecasting platform, the model evaluation across a wide range of cities will

also provide knowledge for global model forecasting and assessment.

In this study, the off-line IAP-AACM is applied to a 1-year simulation for 2014

and the model results of trace gases and aerosol mass concentration are evaluated

against other model datasets and a range of observational datasets, including site

120   observations and satellite data. Firstly we present the global evaluation in section

3.1~3.2. The global budgets of sulfur (dimethylsulfide (DMS), SO_2 and sulfate) and

carbonaceous (organic matter (OM) and black carbon (BC)) aerosol are compared

with other aerosol models in section 3.1. The global distribution and evaluation of

trace gases and aerosol are shown in section 3.2. In section 3.3~3.4, we focus on the

125   model simulation of $PM_{2.5}$ and its components in Chinese cities. The nested

simulation is compared with an abundant dataset of city sites which cover most areas

in China, and the impact of different resolutions on model performance is also

explored. An inter-comparison with the Model Inter-Comparison Study for Asia

(MICS-Asia) models is presented in section 3.3, to give a general comparison across

130   East Asia (EA).

2. Model description and setup

Atmospheric
Chemistry
and Physics
Discussions

2.1 Model description

2.1.1 CAS-ESM

CAS-ESM is the Earth System Model developed by the Chinese Academy of

135   Sciences. It is coupled with the Atmospheric General Circulation Model of IAP

(IAP-AGCM) (Su et al., 2014), the Climate System Ocean Model (LICOM) (Liu et al.,

2012), the Common Land Model (CoLM), the sea ice model (CICE), the Dynamic

Global Vegetation Model of IAP (IAP-DGVM) (Zhu et al., 2018), the IAP-AACM,

and the land and ocean biogeochemical models of IAP (IAP-OBGCM). The

140   IAP-AACM provides mass concentration of trace gases and aerosols for CAS-ESM

and thus provides the corresponding climate effect through the two-way feedback of

aerosols. Currently, global climate and ecological environment change is not only one

of the core issues of international climate and environment diplomacy, but also an

important factor governing the sustainable development of China. Earth system model

145   is a basic tool to understand and solve these problems. The resolution of the

CAS-ESM is $1°×1°$ currently and later will be updated to $0.25°×0.25°$. The CAS-ESM

will calculate a climate numerical experiment with high resolution for 100 years

(1950 ~ 2050) and provide simulation results for the sixth IPCC assessment report and

CMIP6.

150   2.1.2 IAP-AACM

The IAP-AACM is developed on the basis of the Nested Grid Air Quality

Prediction Model System (NAQPMS) (Wang et al. 2006b) and the Global Nested

Grid Air Quality Prediction Model System (GNAQPMS) (Chen et al., 2015).

Atmospheric
Chemistry
and Physics
Discussions

NAQPMS/GNAQPMS is widely used in the simulation of dust (Li et al., 2012),

155   ozone (O_3) (Wang et al., 2006a; Li et al., 2007), deposition (Ge et al., 2014), air

pollution policy control (Wu et al., 2011; Li et al., 2016; Wei et al., 2017) and the

global transportation of mercury (Chen et al., 2015).

Like GNAQPMS, the IAP-AACM is a multi-scale nested model that describes

atmospheric chemistry and aerosol process on both global and regional scales. In the

160   IAP-AACM, sea salt and dust are emitted as dynamic sources. The dust scheme

originates from the wind erosion model developed by Wang et al. (2000) and

improved by Luo et al. (2006). The simulation of sea salt is based on the scheme of

Athanasopoulou et al. (2008). Dry deposition processes are based on the resistance

model approach of Zhang et al. (2003). The gas-phase chemistry scheme is Carbon

165   Bond Mechanism Z (CBM-Z) (Zaveri et al., 1999) which contains 176 chemical

reactions, 67 reactive species, and 20 species undergo photolysis. The cloud

convection, aqueous chemistry, in-cloud and below-cloud scavenging use the second

generation of Regional Acid Deposition Model (RADM2) (Stockwell et al., 1997).

For aerosols, the thermodynamic equilibrium module ISORROPIA (Nenes et al., 1998,

170   1999) is used to calculate gas-particle partitioning of inorganic aerosols and aerosol

water content. Furthermore, an aerosol microphysics dynamic module (APM) (Yu et

al., 2009) was added to expand the simulation from mass concentration to size

distribution (Chen et al., 2014, 2017). The secondary organic aerosol (SOA) module is

based on the mechanism developed by Strader (1999), considering two anthropogenic

Atmospheric
Chemistry
and Physics
Discussions

Open Access

EGU

175   emission precursors (toluene and other aromatic hydrocarbons) and four bio-emission

precursors (isoprene, monoterpene, etc.) (Li et al., 2011).

In addition, the IAP-AACM includes an updated DMS emission module from

Lana et al. (2011). The DMS concentration in seawater is calculated using 47,313

observations of the Global Surface Waters DMS database

180   (http://saga.pmel.noaa.gov/dms/) and an additional 63 observations in the South

Pacific (Lee et al., 2010). The IAP-AACM also provides a second, simplified

gas-phase chemistry mechanism based on a sulfur-only, chemistry box model. The

simplified sulfur-only scheme is specially designed for CAS-ESM to provide the

major aerosol components (sulfate, OM, BC, dust and sea salt). Retaining aerosols

185   with significant climatic radiative effects while cutting computational load, nitrate and

its chemical reactions are excluded. This approach is common in global aerosol

models such as the Integrated Massively Parallel Atmospheric Chemical Transport

(IMPACT) model (Liu et al, 2005) and GLOMAP (Mann et al., 2010). The simplified

scheme contains sulfur species (SO_2, DMS, and sulfur acid gas (H_2SO_4)), ammonia

190   (NH_3) and hydrogen peroxide. Offline monthly fields of the oxidants hydroxyl radical

(OH), nitrate ion radical (NO_3), O_3 and super oxidation of hydrogen (HO_2), generated

from a simulation of the standard version of IAP-AACM, are read in and interpolated.

Chemical processes in the simplified version are the same as those in the standard

version except for the gas-phase scheme mentioned above. In this paper we focus on

195   evaluating simulations of chemical composition in the standard version model driven

by a global version of Weather Research and Forecasting version 3.3 (WRFv3.3). The

global WRF is an extension of mesoscale WRF that was developed for global weather

research and forecasting applications (Richardson et al., 2007).

2.2 IAP-AACM setup

200   In this study, the simulation region covers the globe at $1°\times1°$ resolution and has a

nested domain over EA at $0.33°\times0.33°$. Vertically, the model uses 20 layers, from the

bottom layer of about 50 m to the model top of 20 km, and about 10 layers are located

below 3 km. The simulation area of the nested domain is shown in Fig. 1. The

synchronous time step is 1800 s. The meteorology input frequency is 6 h in the global

205   domain but 3 h in the nested domain. The simulation period is from December 1st,

2013 to December 31th, 2014, and the first month is spin up time. Boundary

conditions for the nested region are provided by the parent grid. As stratospheric

chemistry is not considered in the IAP-AACM, the top boundary concentrations of O_3,

NO_x and CO are prescribed from the Model for Ozone and Related Chemical Tracers

210   version4 (MOZART-4) (Emmons et al., 2010).

2.3 Emissions

      By integrating data from publicly-released emission inventories, we compiled a

global high-resolution ($0.1° \times 0.1°$) emission dataset with source categories (29

species and 14 sectors) and interpolate it to the model resolution. The benchmark year

215   is 2010. Detailed information on the emissions is shown in Table 1. We note that

volcanic emissions are not yet considered here.

      As a consequence of government control policy included in the Five-Year Plan

(FYP), China has achieved an obvious decrease in air pollution in the past ten years,

Atmospheric
Chemistry
and Physics
Discussions

especially for SO_2. According to an announcement by the Ministry of Environmental

220 Protection of China

(http://www.zhb.gov.cn/gkml/hbb/qt/201507/t20150722_307020.htm), the country

completed the emission reduction task of 12th FYP (2010~2015) ahead of schedule in

2014 with a reduction ratio reaching by 12.9%. As the FYP controls suppressed SO_2

emissions mainly in the energy and industry sectors, we adjusted the total SO_2

225 emission for 2014 by a factor of 0.9 in China. The annual mean SO_2 emission is

shown in Fig. 1.

2.4 Meteorology and evaluation

As noted in 2.1.2, meteorological fields were provided offline by the WRFv3.3.

The temporal and horizontal spatial resolution of WRFv3.3 was consistent with

230 IAP-AACM. The atmosphere was divided into 27 vertical layers up to 10 hundred

Pascal (hPa). WRF was driven by the National Centers for Environmental Prediction

(NCEP) Final Analysis (FNL) data.

To understand the model performance overall, a comparison of annual mean

meteorological fields (temperature, wind and relative humidity) between WRF and

235 reanalysis data (National Centers for Environmental Prediction Reanalysis 1

(NCEP-R1)) are presented in Fig. 2. 443 surface sites in the nested domain are also

analyzed with the National Climate Data Center (NCDC) data and the statistical

parameters are shown in Table 2. A comparison of annual mean precipitation between

the model and reanalysis data from the Global Precipitation Climatology Project

240 (GPCP)) is also shown in Fig. S1. Globally, as shown in Fig. 2, the difference in

Atmospheric
Chemistry
and Physics
Discussions

temperature at 2 m (T_2) and wind at 10 m (W_{10}) between the model and observation is

within 2 °C and 2 m s^{-1} respectively, except in high-latitude areas. The relative

humidity at 2 m (RH_2) is generally underestimated on land and overestimated over the

ocean, but the difference in most areas is within ±10%. The difference in precipitation

245   is within 2 mm day^{-1} except in equatorial regions. The frequently strong convection in

tropical areas is difficult to reproduce in the model. The agreement in T_2 and RH_2 with

observations is better than that of W_{10}, with annual correlation coefficients (R) of 0.98,

0.84 and 0.53, respectively. Generally, the meteorology calculated by WRF is similar

to observations.

250   **2.5 Observation data**

Trace gas observation data for CO, O_3, SO_2, and NO_2 in this paper are collected

from   the   World   Data   Center   for   Greenhouse   Gas   (WDCGG)

(http://ds.data.jma.go.jp/gmd/wdcgg/cgi-bin/wdcgg/catalogue.cgi),   the   Acid

Deposition   Monitoring   Network   in   East   Asia   (EANET)

255   (http://www.eanet.asia/product/index.html#datarep),   and   the   Chinese   National

Environmental   Monitoring   Center   (CNEMC)   (http://www.cnemc.cn).   Annual

observation data of particle and aerosol species are from the European Monitoring and

Evaluation Program (EMEP) (http://www.emep.int/), EANET, the United States

Environmental   Protection   Agency   (EPA)

260   (http://aqsdr1.epa.gov/aqsweb/aqstmp/airdata/download_files.html#Daily)   and   the

Interagency Monitoring of Protected Visual Environments (IMPROVE) network

(http://vista.cira.colostate.edu/improve/). As there is a lack of observations of BC and

Atmospheric
Chemistry
and Physics
Discussions
Open Access
EGU

organic carbon (OC) in Asia in 2014, we collected earlier site results from the China

Atmosphere Watch Network (CAWNET) from Zhang et al. (2008). Hourly air quality

265   data in China are downloaded from CNEMC. The other aerosol observations in China

are collected from monitoring sites of Nanjing and Wuhan, and scientific observation

at Xinzhou and Beijing (Chen et al., 2015). Aerosol Optical Depth (AOD) data from

the Moderate Resolution Imaging Spectroradiometer (MODIS) is used to evaluate the

simulated AOD. All these datasets are for 2014, except that the WDCGG is used as an

270   average of 2006~2015 and the CAWNET is for 2006. The observation datasets are

summarized in Table 3 and detailed information of the observation sites is given in

Table S1. Note that the observed species in Table 3 are not always available at the

corresponding sites.

To focus on the severe haze problem in China, and to investigate the model

275   performance over China in more depth, we selected 89 stations in 12 cities

representing typical areas in China. The 12 cities are Beijing, Tianjin, and Langfang

(representing North China, NC), Shanghai, Nantong, and Yancheng (representing

Yangtze River Delta, YRD), Guangzhou and Zhongshan (representing Pearl River

Delta, PRD), Urumqi (representing Northwest China, NWC), Zhengzhou and Wuhan

280   (representing Central China, CC) and Chengdu (representing Southwest China, SWC)

(shown in Fig. 1). The daily mean city-averaged concentration of pollutants are

displayed in figures and used to calculate statistics. In addition, we collected the mass

concentrations of BC, OM, sulfate, nitrate and ammonium in Beijing, Xinzhou,

Nanjing and Wuhan (also shown in Fig. 1) to evaluate the model performance in

Atmospheric
Chemistry
and Physics
Discussions

285   simulating aerosol components.

3 Model results and evaluation

3.1 Budgets

On account of the significant radiative effect of sulfate and carbonaceous aerosols,

their budgets play an important role in the climate change (Penner et al., 1998). So

290   here we elucidate the budgets of sulfate with its precursor gases (DMS and SO_2) and

carbonaceous aerosols.

The global sulfur budgets for DMS, SO_2 and sulfate in IAP-AACM are

summarized in Table 4, along with results from other global aerosol models including

IMPACT (Liu et al., 2005), Goddard Institute for Space Studies General Circulation

295   Model with TwO-Moment Aerosol Sectional (GISS-TOMAS) (Lee et al., 2010),

Atmospheric Chemistry and Climate Model Intercomparison Project (ACCMIP)

models (Lee et al., 2013) and the AeroCom models (Textor et al., 2006). The DMS

emission (23.3 TgS yr^{-1}) is within the range of other models (10.7~23.7 TgS yr^{-1}).

Note that the dry deposition of DMS is zero in IAP-AACM so the sink is just

300   oxidation. This treatment is common in some other models such as ModelE2-TOMAS

and ModelE2-OMA (Lee et al., 2015). As a result, we have a higher burden of DMS of

0.19 TgS, just outside the range (0.05~0.15 TgS), and a longer lifetime of 3 days. For

SO_2, the emissions are a bit lower than the reference range (54.3 TgS yr^{-1} vs.

63.4~94.9 TgS yr^{-1}), and this is ascribed to the lack of volcanic emissions. The

305   volcanic emissions used in most models is based on the work of Andres and Kasgnoc

(1998) and Dentener et al. (2006), in which the average flux for SO_2 is about 12.5 TgS

Atmospheric
Chemistry
and Physics
Discussions

yr^{-1} including continuous degassing and explosive volcanoes. We also note that the benchmark year of the anthropogenic emissions used in the reference models is as early as 2000 or 1990, but that anthropogenic emissions in IAP-AACM are for 2010,

310 which may explain some of the discrepancy. The oxidation of DMS to SO_2 is 22.8 TgS yr^{-1}, within the range of other models' results. The aqueous-phase process is responsible for 61% of the oxidation to sulfate and gas-phase processes are responsible for the remaining 39%. Although it's a bit lower conversion efficiency for aqueous-phase chemistry compared with other models (about 70% ~ 80%), both

315 aqueous phase and gas phase oxidation are well within the range of other models. The SO_2 burden is at the high end of the reference range, because the aqueous-phase oxidation rate for SO_2 is higher than that in the gas-phase (Liu et al., 2005). Due to an inefficient removal in aqueous-phase oxidation (29.8 Tg S) and wet deposition (shown in Table 4 as zero), the lifetime of SO_2 in the model is a little longer than other models

320 (3 days vs. 0.6~2.6 days). In IAP-AACM, the emission of H_2SO_4 is assumed as 2.5% of the total sulfur emission. With a strong wet scavenging effect, 94% of sulfate is removed by wet deposition and the rest by dry deposition.

Table 5 presents the budgets for OM and BC with a range of results from other models including Liu et al. (2005), Lee et al. (2013), Lee et al. (2015), Textor et al.

325 (2006), and those listed in Liu et al. (2005). For the same reasons described above, the emissions of BC/OM are at the low end compared with other models (BC: 7.42 TgS yr^{-1} vs. 7.4~19.0 TgS yr^{-1}; OM: 56.7 TgS yr^{-1} vs 34~144 TgS yr^{-1}). The ratio of dry deposition to wet deposition for BC and OM is 15.8% and 13.6%, respectively. Both

Atmospheric
Chemistry
and Physics
Discussions

the burden and lifetime of carbonaceous aerosol are within the other models' results.

330   The burden of BC and OM is 0.13 Tg and 1.16 Tg respectively and the lifetime is 6.4

days and 7.4 days respectively.

3.2 Global distribution and evaluation

3.2.1 Trace gases

Global annual-averaged surface-layer trace gas distributions from IAP-AACM

335   are evaluated against site observations in Fig. 3. Scatter plots of observation and

simulation data divided into 11 different geographical regions are exhibited in Fig. 4

and the corresponding Normalized Mean Bias (NMB) are shown in Table 6. The 11

geographical regions include Africa, Antarctica, Arctic Ocean, Asia, Atlantic Ocean,

Europe, Indian Ocean, North America (NAmerica), South America (SAmerica),

340   Oceania and Pacific Ocean. Fig. 5 shows the comparison of annual surface

concentrations of CO, O_3 and NO_2 between IAP-AACM and some HTAP atmospheric

chemical models including CAM-Chem (Lamarque et al., 2012), OsloCTM3 (Søvde

et al., 2012), and CHASER(Sudo et al., 2002).

Overall, the global surface CO simulation of IAP-AACM is lower than

345   observations, especially in natural source regions. Antarctic continents and oceans

have the largest difference between site and model as shown in Fig. 3, and the

difference can reach ~100 ppb. Fig. 4 also reveals a significant underestimation in

ocean areas, with NMB ranging from -0.59 to -0.45 shown in Table 6. Over

anthropogenic source regions, by and large, the model is consistent with site data in

350   eastern NAmerica, EA, and the coastal areas of SAmerica and Africa, but is about 50

Atmospheric
Chemistry
and Physics
Discussions

ppb lower in western NAmerica and Europe. The scatter plot clearly shows a negative

bias between the model and observations, especially over the ocean. The lower model

results may be caused by underestimated emissions or overestimated OH. For AACM,

the tropospheric (200 hPa to the surface) mean OH derived by the model is 10.6×10^5

355 molec cm^{-3}. This value agrees well with a study of 14 models for 2000 by Voulgarakis

et al. (2013), where the mean OH concentration was estimated to be $11.1 \pm 1.8 \times 10^5$

molec cm^{-3}. On the other hand, the anthropogenic emission is 546.4 Tg yr^{-1}, lower

than some other emission inventory (e.g. ACCMIP with 610.5 Tg yr^{-1}) (Badia et al.,

2017). Janssens-Maenhout et al. (2015) pointed out that CO emission from HTAPv2

360 has an uncertainty of 15~100% and 35~150% in data from well maintained countries

and poorly maintained countries respectively. Furthermore, the underestimation of CO

is common in other models. Shindell et al. (2006) evaluated 26 global models and

showed that all the model results are lower than observations in the North Hemisphere

(NH) except in the tropics, and it is concluded that this is related to a lower CO

365 emission source. The spatial distribution of CO concentrations in IAP-AACM is

similar to that in other models from HTAP in 2010. High values are found in

industrial areas such as NAmerica, Europe and EA, and biomass burning areas such as

South Africa (SAfrica) and SAmerica. The other models also display lower CO

concentrations over ocean as in IAP-AACM.

370   As displayed in Fig. 3 and Fig. 4, the O_3 spatial distribution simulated by

IAP-AACM is in a good agreement with observations. The O_3 simulations at most

sites are within a factor of two of the observation and the majority of regions have a

17

Atmospheric
Chemistry
and Physics
Discussions

NMB within ± 0.2 (Table 6) except for Africa, Antarctica and Asia. It is worth noting that the annual concentrations of O_3 at the three sites in Southeast Asia are more than

375 twice the observed values. As the sites are coastal, it may be not representative of the wider region simulated by the model. On the other hand, South Asia is a high-emission area for biogenic VOCs. Uncertainty in the biogenic source inventory may also cause large errors in O_3 simulation due to photochemical processes. The model shows a good skill in capturing the seasonal variation of surface O_3 in different

380 regions, as shown in Fig. 6. In the NH, the maximum O_3 concentration occurs in spring or summer on land but over the sea the value is higher in spring and lower in summer. In contrast, higher values occur in autumn or summer in the Southern Hemisphere (SH). The model results match the seasonal cycle both in the trends and the concentration over the ocean in the NH and in the SH very well, with only a small

385 underestimation in Antarctica. However, there is a positive bias during July-September over the land in the NH (NAmerica, Europe and Asia). A similar overestimation occurs in the evaluation of NMMB-MONARCH by Badia et al. (2017). They suspect this may be caused by a reduction of the NO_x titration effect in the summer, which leads to corresponding lower O_3 concentrations in highly

390 industrialized regions. The horizontal distribution of O_3 in IAP-AACM is generally similar to that in other models, as shown in Fig. 5. High concentrations mainly occur downwind of highly polluted areas due to the NO_x titration mentioned above. The model exhibits a higher concentration in the source regions and a lower concentration downwind. However, the model result is in good agreement with observations over

Atmospheric
Chemistry
and Physics
Discussions

395   the ocean, as shown in Fig. 6. The difference in O_3 between models may partly be

related to the dry deposition scheme used by the model. We show the dry deposition

velocity (mainly 0.04 ~ 0.05 cm s^{-1} on water surface) of O_3 in IAP-AACM in Fig. S2.

In the common parameterization $v_d = \frac{1}{r_a+r_b+r_c}$, the canopy resistance r_c is the

dominant term for O_3 dry deposition to water surfaces (Luhar et al., 2017). It is

400   commonly assumed that r_c for water is constant ($\approx$ 2000 s m^{-1}) (Wesely, 1989) and

this is used by default in many global models including CAM-Chem. Based on this,

we do not believe there are large differences in dry deposition between IAP-AACM

and the other models.

NO$_2$ is limited to continental source regions due to human activities. IAP-AACM

405   captures the spatial characteristics well, see Fig. 3. Concentrations in NAmerica,

Europe, and most parts of EA are in good agreement with observations. As shown in

Fig. 4, simulation results are within a factor of two of the observations at most sites

except for a few sites in China where they are underestimated (NMB of -0.59). As we

use the same anthropogenic emission inventory, the spatial distribution of NO$_2$ in NH

410   from IAP-AACM and other models is similar, as shown in Fig. 5. The maxima in the

NH are located in industrial areas due to fossil fuel combustion, and the concentration

of NO$_2$ is much higher in eastern China (>20 ppb) than that in eastern NAmerica and

Europe (3-10 ppb). The maxima in the SH are located in SAmerica and South Africa

due to biomass burning, where NO$_2$ is 1-10 ppb, slightly lower (~3 ppb) than the other

415   models shown in Fig. 5, probably related to the different biomass burning inventory

used (GFED3 vs. GFED4) (Janssens-Maenhout et al., 2015). The concentration over

Atmospheric
Chemistry
and Physics
Discussions

the ocean is lower than 0.1 ppb except at 30 N~60 N, since the source of NO_2 over

the ocean is small, mainly emitted by ships.

Similar to NO_2, SO_2 is high in the NH and low in the SH. The source of SO_2 over

420   the ocean is mainly DMS oxidation from marine organisms while the source over land

is mainly fossil fuel combustion. Maximum concentrations are mainly found in

NAmerica, Europe, India and EA. As a result of environmental protection policies

lagging behind industrial development, SO_2 concentrations in India and China can

reach 15-20 ppb, much higher than that in the US or Europe. As shown in Fig. 3, the

425   IAP-AACM calculates a distribution of 0.1-20 ppb in EA and 0.1-5 ppb in western

NAmerica, which is consistent with observations. The simulation of SO_2 in eastern

NAmerica and Europe is about 1-10 ppb, both of which are overestimated with

NMB=3.52 and NMB=0.52 respectively, as shown in Table 6.

3.2.2 Aerosol composition

430   Fig. 7 and Fig. 8 show the annual surface concentrations of aerosol and $PM_{2.5}$ in

IAP-AACM in comparison with site observations in Europe, NAmerica and Asia. The

corresponding NMB in different regions are also displayed in Table 6. Overall,

aerosol simulations are consistent with site datasets.

As shown in Fig. 7, Sulfate, Nitrate and Ammonium (SNA) are mainly distributed

435   in NH due to their close association with human activities. Sulfate is reproduced

accurately at most sites. The model result is consistent with site records in Asia and

Europe and the simulations at most sites here are within a factor of two of

observations as shown in Fig. 8, with NMB of 0.36 and 0.11 respectively. In America,

the simulation of sulfate is about 2 μg m^{-3} higher than observations. This is consistent

440   with the high level of SO_2 in the eastern America described previously, as the

precursor of sulfate. The simulation of nitrate over the land is more uncertain due to

the complex photochemical reactions of NO_x, but our model reproduces the nitrate

distribution overall. The simulation is close to observation in America but

overestimates it in Europe. There is an underestimation of ~5 μg m^{-3} in Southeast Asia

445   and Japan. Even so, the NMBs are within ±0.8 (the NMB of America, Europe and

Asia is 0.5, 0.74 and -0.61 respectively). Generally, the simulation of ammonium is

comparable to observations in America and most parts of Asia, with an NMB of -0.46

and 0.85 respectively. But there is a positive bias in Europe with an overestimation of

about ~4 μg m^{-3}.

450   For carbonaceous aerosols, there are high values in developing countries or

regions as biomass burning and fossil fuel combustion dominate the sources.

SAmerica and SAfrica contribute most of biomass combustion emissions, and

developing countries (e.g. China and India) where industrial emission controls are less

well implemented contribute most of fossil fuel emissions. BC and OC are low in

455   America and Europe, with values of ~1 μg m^{-3} and ~3 μg m^{-3} respectively. By and

large, the model results are consistent with observations in the three regions shown in

Fig. 8, with the NMB of BC within ±0.65 and OC within ±0.7. The simulations of

both BC and OC are highly consistent with the IMPROVE dataset in America as well

as with the EMEP dataset in Europe. The accuracy of the simulation mainly depends

460   on the emission source, since BC is quite inert to chemical reactions. The simulation

Atmospheric
Chemistry
and Physics
Discussions

of BC in China is accurate with 70% of the stations within a factor of two of observation while OC is underestimated by about 5-10 μg m^{-3}, mainly due to the decrease in emissions from 2006 to 2014 due to the government's pollution control policy (Zheng et al., 2018).

465   Generally, the model shows good skill in simulating PM$_{2.5}$. Model results at most sites are close to observation as shown in Fig. 7, especially in Europe and Asia with NMB of -0.35 and -0.36 respectively. The underestimation in urban areas in western China may be related to uncertainty of emissions.

3.2.3 Comparison with satellite data

470   In order to evaluate the simulation of aerosol in IAP-AACM above the surface, we compared the aerosol optical depth (AOD) of IAP-AACM with MODIS satellite data. The calculation of light-extinction coefficient, b_{ext550} (1/Mm, at 550nm), follows equation (1) given by Li et al. (2011):

$$b_{ext550} = 3.0 \times f_{SNA}(RH)\{[(NH_4)SO_4] + [(NH_4)NO_3]\} + 4.0 \times [OC] \\ + 10.0 \times [LAC] + 1.0 \times [FD] + 0.6 \times [CD] + 1.7 \times f_{ss}(RH) \times [SS] \tag{1}$$

475   where $f_{SNA}(RH)$ and $f_{SS}(RH)$ represent the hygroscopic growth factor for SNA and sea salt respectively, and the variables in brackets are the mass concentration of aerosol species (OC: organic carbon; LAC: light-absorbing carbon; FD: fine dust; CD: coarse dust; SS: sea salt).

      Fig. 9 shows the comparison of AOD between IAP-AACM and MODIS for each

480   season in 2014. In general, the model AOD reproduces the spatial features of aerosol exhibited by satellites globally. For example, the high value around 60 °S, ranging from 0.1 to 0.3, is due to high concentrations of sea salt. The maximum in SAmerica

22

Atmospheric
Chemistry
and Physics
Discussions

and SAfrica is due to the large amount of carbonaceous aerosol produced by biomass

burning. The desert maximum over 0.5 is caused by mineral dust in NAfrica, Arabian

485   Peninsula and western China. High AOD in NAmerica, Europe, India, and EA is

caused by anthropogenic aerosols. Furthermore, there is a good agreement of the

seasonal variations with satellite observations. For example, the AOD in the desert

areas of NH reaches a maximum in March-April-May (MAM) since this is the season

with frequent dust storms. SAmerica and SAfrica have lowest AOD in the

490   September-October-November (SON) season as there is less biomass burning in this

season. The east of China has highest AOD in December-January-February (DJF), as

the country suffers severe haze at this time. However, there are several biases between

model and satellite. The model shows a weaker AOD in Southeast Asia than

observation where the value is mainly controlled by biomass burning. The AOD from

495   IAP-AACM is also lower than observation to about ~0.4 in eastern China, mainly due

to the negative bias of anthropogenic aerosols.

3.3 Nested simulation evaluation

3.3.1 Distribution and evaluation in EA

Fig. 10 shows the annual distribution of the four pollutants SO_2, NO_2, PM_{10} and

500     $PM_{2.5}$, against 45 city stations from the nested simulation. In general, the simulation

shows better agreement with sites in Eastern China than Western China. Model results

for NO_2 concentration are a little low, probably due to an underestimation of the

emissions, while SO_2, PM_{10} and $PM_{2.5}$ are highly consistent with observations. The

model values of PM_{10} and $PM_{2.5}$ include dust aerosol in Fig. 10, and dust contributes a

23

Atmospheric
Chemistry
and Physics
Discussions

505   lot to particles in North China. In the following discussion of $PM_{2.5}$, we focus on

primary $PM_{2.5}$, BC, OC, SNA and SOA. The distribution of $PM_{2.5}$ and its precursors

show high levels in the East and low in the West, which is related to urbanization and

industrialization. Despite good agreement with observations in most places, the

concentration in Tibet is greatly underestimated.

510   Unlike global models, regional models need boundary conditions and total mass

in a region is not conserved. The physical and chemical processes are relatively

complex, with higher spatio-temporal resolution and more computationally-intensive.

Here a comparison between IAP-AACM and several regional models of MICS-Asia is

presented in Fig. 11. The MICS-Asia models included here are WRF-Chem (Tuccella

515   et al., 2012), CMAQ (Mebust et al., 2003) and NAQPMS (Wang et al., 2006). Their

simulations are for 2010 with the same meteorological fields and emissions, and the

horizontal resolution is 45 km. As shown in Fig. 11, the nested simulation of

IAP-AACM has consistent spatial distribution of pollutants in the far northwest of the

domain, which cannot be reproduced in the regional models. The fixed boundary

520   conditions are responsible for this phenomenon, for there is no transportation from

upwind of the boundary. Overall, the IAP-AACM shows similar annual distributions

to MICS-Asia models in EA, as the emission inventory used in IAP-AACM is largely

the same as MICS-Asia models. But concentrations in IAP-AACM are slightly lower

in China and Japan, especially for NO_2 and $PM_{2.5}$. Furthermore, NAQPMS shows

525   stronger transportation downwind of the continent. As the regional version of

IAP-AACM, NAQPMS has the same dynamic framework and physicochemical

processes as IAP-AACM, but the meteorology conditions are not the same.

3.3.2 Trace gas evaluation in cities

To get deeper insight into the performance of IAP-AACM in cities, a nested

530   simulation was compared with daily averaged observations in 12 cities across China.

We first focus on NO_2 and SO_2 since they are precursors of SNA aerosols. The

monthly variation of SO_2 and NO_2 against observations is shown in Fig. 12 and Fig.

13. Three-quarters of cities show an annual concentration of NO_2 of around 50 μg m^{-3},

twice as high as SO_2 in summer and autumn, owing to the tougher SO_2 emission

535   reduction policy implemented since 2005. For SO_2, the model shows good agreement

with observations except in Wuhan as shown in Fig. 12. This probably implies an

overestimation of emissions in this city. Furthermore, IAP-AACM reproduces the

seasonal variation well, showing good comparison to observations with R over 0.5 in

most cities. In particular, the cities in NC have a high R in the range 0.76-0.89.

540   As illustrated in Fig. 13, the model shows a good performance for NO_2 in most

cities, especially in YRD, PRD and SWC. The statistics summarized in Table 7 clearly

show that the model captures the monthly variations well, with R of 0.49-0.7 in NC,

YRD and PRD, and matches the observations well with Root Mean Square Error

(RMSE) typically less than 20 μg m^{-3} in SWC and PRD. Overall, the model results are

545   more likely to be overestimated in NC, YRD and CC in summer. As the "NO_2" values

reported by routine monitoring sites are NO_2^*, which partially includes HNO_3 and

NO_3^-, it is common to underestimate the observed "NO_2". Here we also give a

comparison of NO_2 column concentration between model and satellite observations

25

Atmospheric
Chemistry
and Physics
Discussions

from GOME-2A in Fig. S3. Generally, there is a good agreement in NO_2 column

550   concentration in China in different seasons. The model significantly underestimates

concentrations in Urumqi, probably as a consequence of uncertainties in emissions. In

brief, the nested forecasting generally captures the seasonal variation of NO_2 with R

near or above 0.5 in NC, YRD and PRD, but shows a poorer performance in the other

parts of China.

555   3.3.3 Aerosol composition evaluation in cities

As shown in Fig. 14, the model performs very well in the simulation of $PM_{2.5}$.

Statistics are shown in Table   7. The model reproduces $PM_{2.5}$ trends over the 12

cities well, particularly in NC, YRD and SWC, with an R of 0.70-0.79, 0.71-0.80 and

0.77 respectively. The model results are close to or slightly lower than site

560   observations. The concentration in NC on some winter days is below the observations.

This underestimation of $PM_{2.5}$ in severe haze periods is common in atmospheric

chemistry models, mainly as a result of the deficiency in the SNA and Secondary

Organic Aerosol (SOA) simulation (Zheng et al., 2015; Donahue et al., 2006). Besides,

there is a clear underestimation in PRD and Urumqi where mean values are less than

565   half of the observations, with NMB around -0.5. This is partly caused by the

underestimation of emission sources, as NO_2 is lower in these cities. Furthermore,

dust plays an important role as a component of $PM_{2.5}$ in Urumqi, and this is not

included in the result. For these reasons, we investigate the aerosol simulation in

further detail below.

570   To assess the performance of IAP-AACM in representing aerosol components,

26

Atmospheric
Chemistry
and Physics
Discussions

we compared the model results with 4 stations in NC, YRD and CC in Fig. 15. Generally, the model represents the variation of BC well with R ranging from 0.5 to 0.8 and the value get close to observations. As a primary specie, it is probably on account of its emission inventory. Unlike BC, there is an underestimation of OM at

575   the four stations, with a difference of 8-12 $\mu g\ m^{-3}$. For SNA aerosols, the model also underestimates observations. Sulfate is close to observations in the northern cities (Beijing and Xinzhou), but is underestimated in southern and central cities (Nanjing and Wuhan) by about 10 $\mu g\ m^{-3}$, with R from 0.4 to 0.6. As noted above, the concentration of SO_2 in Wuhan is overestimated. This suggests the sulfur oxidation

580   may be insufficient. This insufficient conversion has been discussed widely in recent years (Cheng et al., 2016; He et al., 2014). Moreover, SO_2 discharged by coal power plants plays a vital role in the formation of sulfate. The coarse grid resolution is insufficient to reproduce the rapid conversion of H_2SO_4 to particles in the plume. The gas-phase oxidation (SO_2 + OH → H_2SO_4(g)) is very sensitive to meteorological

585   variables (particularly radiation and temperature) and gas (OH and NOx) concentration around the stacks (Stevens et al., 2012). This may lead to a local discrepancy between simulation and observation. The results for ammonium show similar characteristics. The simulation of nitrate is highly underestimated with R ranging from 0.3 to 0.5. The underestimation is due to a high frequency of 'zero'

590   value in daytime of summer and autumn. This is due to the sensitivity of nitrate to temperature in the thermodynamic equilibrium module which leads to decomposition to NO_2. This also leads to overestimation of NO_2 as shown in in Fig.13. Schaap et al.

Atmospheric
Chemistry
and Physics
Discussions

(2011) found the same phenomenon in the LOTOSEUROS model using ISORROPIA

and recommended improvements in the equilibrium module, including coarse mode

595   nitrate. In other respects, the model can reproduce aerosol components reasonably

well in these cities

3.4 Global versus regional results

To evaluate the improvements due to higher model resolution, we compare the

global simulation ($1°\times1°$) with the nested simulation ($0.33°\times0.33°$) over China. Table

600   7 gives the statistics of $PM_{2.5}$, SO_2 and NO_2 simulated at the different resolutions. The

nested domain can effectively improve the simulation of city pollutants, especially

$PM_{2.5}$, because high-resolution grid can provide better resolved emissions and

meteorological fields in urban and rural areas. As shown in Table 7, the correlation

coefficients of the three species in the nested simulations are significantly higher than

605   in the global simulations. The RMSE of the nested results in most cities are reduced.

For $PM_{2.5}$, the correlation at high resolution rises in all the cities except Shanghai, and

the PRD has the most significant increase. The R for Guangzhou and Zhongshan

increase by 0.2 and 0.25 respectively, and the R for Urumqi increases by 0.19.

Moreover, the RMSE decreases over 9 cities. The impact of the nested grid on

610   simulation of SO_2 is clear, with R increasing over 8 cities getting R raised and RMSE

reducing over 9 cities. In particular, the simulation in NC, YRD and SCW improves

significantly, with better representation of monthly variation and closer comparison to

observations. For NO_2, the R significantly increases in 9 cities (all except Shanghai,

Nantong and Wuhan) and RMSE decreases in 7 cities. The best performance is in

28

Atmospheric
Chemistry
and Physics
Discussions

615 Beijing where there is an improvement of R from 0.48 to 0.68.

4. Conclusions

A global-nested aerosol and atmospheric chemistry model coupled into CAS-ESM is introduced in this study. The aim is to provide more precise information on climate effects and air pollution on both global and regional scales. In IAP-AACM,

620 the emissions of sea salt, dust and DMS are calculated online. Gas-phase chemistry includes both the CBM-Z module and a simplified reaction scheme without nitrate chemistry specifically for CAS-ESM. Aqueous chemistry and wet deposition are calculated by RADM, and the dry deposition scheme is from Zhang et al. (2003). The aerosol module contains ISORROPIA and the scheme of Strader et al. (1999). Here

625 we concentrate on the evaluation of the standard version of IAP-AACM driven by WRF offline. The difference between the simplified and standard versions driven by WRF and the difference between the simplified version driven by IAP-AGCM (online) and WRF (offline) will be presented in our next work.

For the global simulation, the surface distribution of trace gas in the model agrees

630 reasonably well with site observations, mostly within a factor of two. Like other models, IAP-AACM underestimates CO over the oceans, mainly due to the underestimation of emissions over the sea. The model reproduces the spatial variation of O_3 well, with a range of 30-70 ppb at $30\,°\,S\sim60\,°\,N$. Furthermore, the model represents the seasonal variation of O_3 globally, with only a slightly overestimation in

635 summer over the land in NH. The simulation of NO_2 is consistent with both site records and other models. For SO_2, it shows a good agreement with observation

except for an overestimation in eastern America and Europe. With a weak scavenging

rate by deposition and oxidation, SO_2 in the model has a longer lifetime (3 days)

compared with other models (0.6-2.6 days) and the burden (0.63 Tg S yr^{-1}) is at the

640   high end of the range 0.2-0.69 Tg S yr^{-1}. The budgets of both carbonaceous aerosols

and sulfate are similar to those in other models. At the surface, IAP-AACM shows

very close comparison to observations for BC and OC but more variable performance

for SNA. In general, the simulation matches records on sulfate (NMB=0.36) in Asia

and on nitrate and ammonium (NMB within ±0.5) in America. But it overestimates

645   sulfate and ammonium (NMB=1.1 and 1.49 respectively) in Europe and overestimates

only sulfate (NMB=1.94) in America. Above the surface, IAP-AACM captures the

broad seasonal and spatial features of AOD shown in the MODIS.

For the nested simulation, IAP-AACM shows a very similar annual distribution

over EA and a more reasonable distribution on the boundary, compared with regional

650   models from the MICS-Asia project. IAP-AACM shows a good agreement with site

data from Chinese cities for both surface concentration and monthly variation. The

model compares well with observations of NO_2 and SO_2, especially in NC and YRD.

In most cities, IAP-AACM shows very good simulation skill for $PM_{2.5}$, not only for

the monthly variation, but also for daily variability, with R near or above 0.7. For

655   aerosol compositions, BC simulation shows better correlation coefficients (above 0.5)

in all four cities. The simulation of OM is lower than observations. The model results

of sulfate and ammonium in North China are close to observations, but it

underestimates in South China. As nitrate is easily decomposed at high temperatures

Atmospheric
Chemistry
and Physics
Discussions

in the model, it is significantly underestimated in summer and autumn. The

660 comparison of global (1°×1°) and nested (0.33°×0.33°) results indicates that the

model reproduces the spatial variation of pollutants in the city significantly better at

fine resolution, as there are huge differences between urban and country in

meteorological field and emission.

In general, the model results for trace gases and carbonaceous aerosols show a

665 favorable performance. Nevertheless, the simulation of secondary aerosols shows

some weaknesses. To reduce uncertainties in the simulation of SNA, more work is

needed to improve not only aerosol chemistry but also emission inventory. Moreover,

the SOA module is relatively simple, and it could be upgraded to incorporate a

comprehensive scheme (e.g. Volatility Bias Set by Donahue et al. (2006)) and verified

670 with observations.

Atmospheric
Chemistry
and Physics
Discussions

Open Access

EGU

Atmospheric
Chemistry
and Physics
Discussions

References

Akimoto, H.: Global air quality and pollution. Science, 302(5651), 1716, 2003.

685   Andres, R. J., & Kasgnoc, A. D. :A time-averaged inventory of subaerial volcanic sulfur emissions, Journal of Geophysical Research Atmospheres, 103(D19), 25251-25261, 1998.

Athanasopoulou, E., Tombrou, M., Pandis, S. N., & Russell, A. G. : The role of sea-salt emissions and heterogeneous chemistry in the air quality of polluted coastal areas, Atmospheric Chemistry & Physics, 8(19), 5755-5769, 2008.

690   Badia, A., Jorba, O., Voulgarakis, A., Dabdub, D., Pérez García pando, C., & Hilboll, A., et al. : Description and evaluation of the multiscale online nonhydrostatic atmosphere chemistry model (NMMB-MONARCH) version 1.0: gas-phase chemistry at global scale, Geoscientific Model Development, 10, 1-47, 2017.

Calvert, J. G. : SO_2, NO and NO_2 oxidation mechanisms: atmospheric considerations, 1984.

695   Charlson, R. J., S. E. Schwartz, J. M. Hales, R. D. Cess, J. A. Coakley, J. E. Hansen, and D. J. Hofmann , Climate forcing by anthropogenic aerosols, Science, 255, 423– 430, 1992.

Chen, C., Sun, Y. L., Xu, W. Q., Du, W., Zhou, L. B., & Han, T. T., et al. : Characteristics and sources of submicron aerosols above the urban canopy (260 m) in Beijing, china, during the 2014 APEC summit, Atmospheric Chemistry and Physics, 15, 12879–12895, 2015.

700   Chen, H. S., Wang, Z. F., Li, J., Tang, X., Ge, B. Z., & Wu, X. L., et al. : GNAQPMS-HG v1.0, a global nested atmospheric mercury transport model: model description, evaluation and application to trans-boundary transport of Chinese anthropogenic emissions, Geoscientific Model Development, 8(5), 6949-6996, 2015.

Chen X. S., Wang, Z. F., Li, J. et al. : Simulation of particle number size distribution in Beijing in

705   winter using NAQPMS+APM model. (in Chinese), 20 (6): 611−619, doi:10.3878/j.issn.1006-9585.2015.15095, 2015.

Chen, X. S., Wang, Z. F., Yu, F. Q., Pan, X. L., Li, J., & Ge, B. Z., et al. : Estimation of atmospheric aging time of black carbon particles in the polluted atmosphere over central-eastern china using microphysical process analysis in regional chemical transport model. Atmospheric

710   Environment, 163(5): 44-56, 2017.

Cheng, Y., Zheng, G., Wei, C., Mu, Q., Zheng, B., & Wang, Z., et al. : Reactive nitrogen chemistry in aerosol water as a source of sulfate during haze events in china. Science Advances, 2(12), 2016.

Dentener, F., Kinne, S., Bond, T., Boucher, O., Cofala, J., & Generoso, S., et al. : Emissions of primary aerosol and precursor gases in the years 2000 and 1750 prescribed data-sets for aerocom.

715   Atmospheric Chemistry & Physics, 6(12), 4321-4344, 2006.

Donahue N. M., Robinson A. L., Stanier C. O., et al. : Coupled partitioning, dilution, and chemical aging of semivolatile organics. Environmental Science & Technology, 40(8):2635-2643, 2006.

Emmons, L. K., Walters, S., Hess, P. G., Lamarque, J.-F., Pfister, G. G., Fillmore, D., Granier, C., Guenther, A., Kinnison, D., Laepple, T., Orlando, J., Tie, X., Tyndall, G., Wiedinmyer, C.,

720   Baughcum, S. L., and Kloster, S.: Description and evaluation of the Model for Ozone and Related chemical Tracers, version 4 (MOZART-4), Geoscientific Model Development, 3, 43–67, 2010.

Gantt, B., He, J., Zhang, X., Zhang, Y., & Nenes, A. : Incorporation of advanced aerosol activation treatments into CESM/CAM5: model evaluation and impacts on aerosol indirect effects. Atmospheric Chemistry & Physics, 369(13), 32291-32325, 2014.

725   Ge, B. Z., Wang, Z. F., Xu, X. B., Wu, J. B., Yu, X. L., and Li, J. : Wet deposition of acidifying

Atmospheric
Chemistry
and Physics
Discussions

substances in different regions of China and the rest of East Asia: Modeling with updated NAQPMS. Environment Pollution, 187, 10-21, 2014.

Giorgi, F., Bi, X., & Qian, Y. : Indirect vs. direct effects of anthropogenic sulfate on the climate of East Asia as simulated with a regional coupled climate-chemistry/aerosol model. Climatic Change,
730   58(3), 345-376, 2003.

Granier, C., Lamarque, J. F., Mieville, A., Muller, J. F., and Olivier, J.: POET. : a database of surface emissions of ozone precursors, tech. report, available at: http://www.aero.jussieu.fr/projet/ACCENT/POET.php , 2005.

Houghton, J. E. T., Ding, Y. H., Griggs, J., Noguer, M., Pj, V. D. L., & Dai, X., et al. : IPCC 2001.
735   Climate Change 2001: the scientific basis. Climate Change 2001: The Scientific Basis, 2001:227-239, 2001.

He, H., Wang, Y., Ma, Q., Ma, J., Chu, B., & Ji, D., et al. : Corrigendum: mineral dust and nox promote the conversion of so2 to sulfate in heavy pollution days. Sci Rep, 4(1), 4172, 2014.

IPCC (Intergovernmental Panel on Climate Change): Climate Change: The Physical Science Basis.
740   Contribution of Working Group I to the Fourth Assessment, Report of the Intergovernmental Panel on Climate Change, Cambridge University Press, Cambridge, United Kingdom, and New York, NY, USA, 2007.

Janssens-Maenhout, G., Crippa, M., Guizzardi, D., Dentener, F., Muntean, M., & Pouliot, G., et al. : HTAP_v2.2: a mosaic of regional and global emission grid maps for 2008 and 2010 to study
745   hemispheric transport of air pollution. Atmospheric Chemistry & Physics, 15(8), 12867-12909, 2015.

Kaiser, J. C., Hendricks, J., Righi, M., Jӧckel, P.,Tost, H.,Kandler, K., et al. : Global aerosol modeling with MADE3 (v3.0) in EMAC (based on v2.53): model description and evaluation. Geoscientific Model Development Discussion. https://doi.org/10.5194/gmd-2018-185, 2018

750   Kan, H. D., & Chen, B. H. : Analysis of exposure-response relationships of air particulate matter and adverse health outcomes in China. Journal of Environment and Health, 19, 422-424, 2002.

Lamarque, J. F., Emmons, L. K., Hess, P. G., Kinnison, D. E., Tilmes, S., & Vitt, F., et al. : Cam-chem: description and evaluation of interactive atmospheric chemistry in the community earth system model. Geoscientific Model Development, 5(2), 369-411, 2012.

755   Lana, A., Bell, T. G., Simó, R., Vallina, S. M., Ballabrera-Poy, J., & Kettle, A. J., et al. : An updated climatology of surface dimethylsulfide concentrations and emission fluxes in the global ocean. Global Biogeochemical Cycles, 25(1), 3-25, 2011.

Lee, Y. H., & Adams, P. J. : Evaluation of aerosol distributions in the GISS-TOMAS global aerosol microphysics model with remote sensing observations. Atmospheric Chemistry & Physics
760   Discussions, 10(5), 2129-2144, 2010.

Lee, Y. H., Lamarque, J. F., Flanner, M. G., Jiao, C., Shindell, D. T., & Berntsen, T., et al. : Evaluation of preindustrial to present-day black carbon and its albedo forcing from Atmospheric Chemistry and Climate Model Intercomparison Project (ACCMIP). Atmospheric Chemistry & Physics Discussions, 13(5), 2607-2634, 2013.

765   Lee, Y. H., Adams, P. J., & Shindell, D. T. : Evaluation of the global aerosol microphysical ModelE2-TOMAS model against satellite and ground-based observations. Geoscientific Model Development, 8(3), 631-667, 2015.

Li, J. J., Shao, L. Y., & Yang, S. S. : Adverse effect mechanisms of inhalable particulate matters. Journal of Environment and Health, 3, 185-188, 2006.

34

Atmospheric
Chemistry
and Physics
Discussions

770　Li, J., Z. Wang, et al. : "Modeling study of ozone seasonal cycle in lower troposphere over east Asia." Journal of Geophysical Research-Atmospheres, 112(D22), 2007.

Li, J., Wang, Z., Wang, X., Yamaji, K., Takigawa, M., & Kanaya, Y., et al. : Impacts of aerosols on summertime tropospheric photolysis frequencies and photochemistry over central eastern china. Atmospheric Environment, 45(10), 1817-1829, 2011.

775　Li, J., Z. Wang, et al. : "Mixing of Asian mineral dust with anthropogenic pollutants over East Asia: a model case study of a super-duststorm in March 2010." Atmospheric Chemistry and Physics, 12(16): 7591-7606, 2012.

Li, J., Yang, W., Wang, Z., Chen, H., Hu, B., et al. : Modeling study of surface ozone source-receptor relationships in East Asia. Atmospheric Research, 167, 77-88, 2016.

780　Li, J., Du, H., Wang, Z., Sun, Y., Yang, W., & Li, J., et al. : Rapid formation of a severe regional winter haze episode over a mega-city cluster on the north china plain, Environmental Pollution, 223, 605-615, 2017.

Li, J., Chen, X., Wang, Z., Du, H., Yang, W., & Sun, Y., et al. : Radiative and heterogeneous chemical effects of aerosols on ozone and inorganic aerosols over East Asia, Science of the Total
785　Environment, 622, 1327-1342, 2018.

Liu, H., Lin, P., Yu, Y. Q., & Zhang, X. : The baseline evaluation of LASG/IAP climate system ocean model (LICOM) version 2. Journal of Meteorological Research, 26(3), 318-329, 2012.

Liu, X., Penner, J. E., & Herzog, M. : Global modeling of aerosol dynamics: model description, evaluation, and interactions between sulfate and nonsulfate aerosols, Journal of Geophysical
790　Research Atmospheres, 110(D18), 2005

Luhar, A. K., Galbally, I. E., Woodhouse, M. T., & Thatcher, M. : An improved parameterisation of ozone dry deposition to the ocean and its impact in a global climate-chemistry model, Atmospheric Chemistry & Physics, 17(5), 1-40, 2017.

Luo, Y. F., Zhou, X. J., Li, W. L. : Advances in the Study of Atmospheric Aerosol Radiative
795　Forcing and Climate Change. Advance in Earth Sciences, 13(6), 572-581, 1998. (in Chinese)

Luo, G., & WANG Z. F. : A Global Environmental Atmospheric Transport Model (GEATM): Model Description and Validation, Atmospheric Science, 30(3), 504-518, 2006.

The NCEP/NCAR 40-Year Reanalysis Project: March, BAMS, 1996.

Mann, G. W., Carslaw, K. S., Spracklen, D. V., Ridley, D. A., Manktelow, P. T., & Chipperfield, M.
800　P., et al. : Description and evaluation of GLOMAP-mode: a modal global aerosol microphysics model for the UKCA composition-climate model, Geoscientific Model Development, 3(2), 519-551, 2010.

Mathur, R., & Dennis, R. L. : Seasonal and annual modeling of reduced nitrogen compounds over the eastern United States: Emissions, ambient levels, and deposition amounts, Journal of
805　Geophysical Research Atmospheres, 108(D15), 22-1 – 22-15, 2003.

Mathur, R., Xing, J., Gilliam, R., Sarwar, G., Hogrefe, C., & Pleim, J., et al. : Extending the Community Multiscale Air Quality (CMAQ) modeling system to hemispheric scales: overview of process considerations and initial applications, Atmospheric Chemistry & Physics, 17(20), 1-46, 2017.

810　Mebust, M. R., Eder, B. K., Binkowski, F. S., & Roselle, S. J. : Models-3 Community Multiscale Air Quality (CMAQ) model aerosol component 2. model evaluation. Journal of Geophysical Research Atmospheres, 108(D6), 2003.

Nenes, A., S. Pandis, et al. : ISORROPIA: A New Thermodynamic Equilibrium Model for

Atmospheric
Chemistry
and Physics
Discussions

Multiphase Multicomponent Inorganic Aerosols, Aquatic Geochemistry4(1): 123-152, 1998.

815   Nenes, A., S. N. Pandis, et al. : Continued development and testing of a new thermodynamic aerosol module for urban and regional air quality models, Atmospheric Environment33(10): 1553-1560, 1999.

A. Søvde, Prather, M. J., Isaksen, I. S. A., & Berntsen, T. K. : The chemical transport model Oslo CTM3. Geoscientific Model Development, 5(6), 1441-1469, 2012.

820   Penner, J. E., Chuang, C. C. and Grant, K. : Climate forcing by carbonaceous and sulfate aerosols, Climate Dynamics, 14(12), 839-851, 1998.

Penner, J. E., Andreae, M., Annegarn, H., et al. : climate change 2001: the scientific basis, contribution of working group I to the third assessment report of the IPCC, 2001.

Pochanart, P., J. Kreasuwun, et al. : Tropical tropospheric ozone observed in Thailand.
825   Atmospheric Environment, 35(15), 2657-2668, 2001.

Pope III CA, Burnett RT, ThunMJ, Calle EE, Krewski D, Ito K, Thurston GD. Lung cancer, cardiopulmonary mortality, and long-term exposure to fine particulate air pollution. JAMA 287, 1132–1141, 2002.

Price, C., J. Penner, & M. Prather. : NOx, from lightning: 1. global distribution based on lightning
830   physics. Journal of Geophysical Research: Atmospheres, 102(D5), 5929-5941, 1997.

Randerson, J. T., G. R. vander Werf, L. Giglio, G. J. Collatz, and P. S. Kasibhatla. : Global Fire Emissions Database, Version 4, (GFEDv4). ORNL DAAC, Oak Ridge, Tennessee, USA. https://doi.org/10.3334/ORNLDAAC/1293, 2010.

Richardson, M. I., Toigo, A. D. and Newman, C. E: Planet WRF: A General Purpose, Local to
835   Global Numerical Model for Planetary Atmosphere and Climate Dynamics, Journal of Geophysical Research, 112, E09001, doi:10.1029/2006JE002825, 2007.

Saxena, P., and Seigneur, C.: On the oxidation of SO_2 to sulfate in atmospheric aerosols. Atmospheric Environment, 21(4), 807-812, 1987.

Schaap, M., Otjes, R. P., and Weijers, E. P. : Illustrating the benefit of using hourly monitoring
840   data on secondary inorganic aerosol and its precursors for model evaluation. Atmospheric Chemistry & Physics, 11(21), 11041-11053, 2011.

Schneider et al : Evaluating the Hydrological Cycle over Land Using the Newly-Corrected Precipitation Climatology from the Global Precipitation Climatology Centre (GPCC). Atmosphere 8(3), 52; doi:10.3390/atmos8030052, 2017.

845   Shindell, D. T., G. Faluvegi, et al. : Multimodel simulations of carbon monoxide: Comparison with observations and projected near-future changes, Journal of Geophysical Research-Atmospheres111 (D19), 2006.

Shindell, D. T., Lamarque, J. F., Schulz, M., Flanner, M., Jiao, C., & Chin, M., et al. (). Radiative forcing in the ACCMIP historical and future climate simulations, Atmospheric Chemistry &
850   Physics,13(3), 2939-2974, 2013.

Sindelarova, K., Granier, C., Bouarar, I., Guenther, A., Tilmes, S., Stavrakou, T., Müller, J.-F., Kuhn, U., Stefani, P., and Knorr, W. : Global dataset of biogenic VOC emissions calculated by the MEGAN model over the last 30 years, doi:10.5194/acpd-14-10725-2014 , Atmospheric Chemistry & Physics Discussions 14 : 10725-10788, 2014.

855   Søvde, O. A., Prather, M. J., Isaksen, I. S. A., & Berntsen, T. K. : The chemical transport model oslo ctm3. Geoscientific Model Development, 5(6), 1441-1469, 2012.

Stevens, R. G., Pierce, J. R., Brock, C. A., Reed, M. K., Crawford, J. H., & Holloway, J. S., et al. ,

Nucleation and growth of sulfate aerosol in coal-fired power plant plumes: sensitivity to background aerosol and meteorology. Atmospheric Chemistry & Physics, 12(1), 189-206, 2012.

860　Stockwell, W. R., Kirchner, F., Kuhn, M., & Seefeld, S. : A new mechanism for regional atmospheric chemistry modeling, Journal of Geophysical Research Atmospheres, 102(D22), 25847-25879, 1997.

Strader, R., F. Lurmann, et al. : Evaluation of secondary organic aerosol formation in winter, Atmospheric Environment 33(29): 4849-4863, 1999.

865　Sudo, K., Takahashi, M., Kurokawa, J. I., & Akimoto, H. : Chaser: A global chemical model of the troposphere 1. Model description. Journal of Geophysical Research Atmospheres, 107(D17), ACH-1-ACH 7-20, 2002.

Su, T., Xue, F., & Zhang, H. : Simulating the intraseasonal variation of the East Asian summer monsoon by IAP AGCM 4.0, Advances in Atmospheric Sciences, 31(3), 570-580, 2014.

870　Tang Y., Dong, W., Li, L., Xue, W., Wang, B.. : CPL7 and its application prospect in the Earth system models of China, Advances in Earth Science, 30(5):620-625, 2015. (in Chinese)

Tao, J., J. Gao, L. Zhang, R. Zhang, H. Che, Z. Zhang, Z. Lin, et al.: $PM_{2.5}$ pollution in a megacity of southwest China: source apportionment and implication, Atmospheric Chemistry & Physics 14(4):8679-8699, 2014.

875　Textor, C., Schulz, M., Guibert, S., Kinne, S., Balkanski, Y., & Bauer, S., et al. : Analysis and quantification of the diversities of aerosol life cycles within AEROCOM, Atmospheric Chemistry & Physics, 6, 1777-1813, 2006.

Tie, X., Zhang, Q., He, H., Cao, J., Han, S., & Gao, Y., et al. : A budget analysis of the formation of haze in Beijing. Atmospheric Environment, 100, 25-36, 2015.

880　Tie X, Huang R J, Cao J, et al. Severe Pollution in China Amplified by Atmospheric Moisture, Scientific Reports, 7(1):15760, 2017.

Tsigaridis, K., Krol, M., Dentener, F. J., & Balkanski, Y. : Change in global aerosol composition since preindustrial times, Atmospheric Chemistry & Physics, 6(12), 5143-5162, 2006.

Tsigaridis, K., Daskalakis, N., Kanakidou, M., Adams, P. J., Artaxo, P., & Bahadur, R., et al. : The
885　AEROCOM evaluation and intercomparison of organic aerosol in global models, Atmospheric Chemistry & Physics, 14(5), 6027-6161, 2014.

Tuccella, P., Curci, G., Visconti, G., Bessagnet, B., Menut, L., & Park, R. J. : Modeling of gas and aerosol with wrf/chem over europe: evaluation and sensitivity study, Journal of Geophysical Research Atmospheres, 117(D3), 2012.

890　Voulgarakis, A., Naik, V., Lamarque, J.-F., Shindell, D. T., Young, P. J., Prather, M. J.,Wild, O., Field, R. D., Bergmann, D., Cameron-Smith, P., Cionni, I., Collins, W. J., Dalsøren, S. B., Doherty, R. M., Eyring, V., Faluvegi, G., Folberth, G. A., Horowitz, L. W., Josse, B., MacKenzie, I. A., Nagashima, T., Plummer, D. A., Righi, M., Rumbold, S. T., Stevenson, D. S., Strode, S. A., Sudo, K., Szopa, S., and Zeng, G.: Analysis of present day and future OH and methane lifetime in the
895　ACCMIP simulations, Atmospheric Chemistry & Physics, 13, 2563–2587, doi:10.5194/acp-13-2563-2013, 2013.

Wang, L. T., Wei, Z., Yang, J., Zhang, Y., Zhang, F. F., & Su, J., et al. : The 2013 severe haze over the southern Hebei, China: Model evaluation, source apportionment, and policy implications, Atmospheric Chemistry & Physics Discussions, 13(11), 28395-28451, 2013.

900　Wang, Y. X., Mcelroy, M. B., Jacob, D. J., & Yantosca, R. M. : A nested grid formulation for chemical transport over Asia: Applications to CO, Journal of Geophysical Research, 109(D22),

Atmospheric
Chemistry
and Physics
Discussions

2285-2311, 2008.

Wang, Y., Li, L., Chen, C., Huang, C., Huang, H., & Feng, J., et al. : Source apportionment of fine particulate matter during autumn haze episodes in Shanghai, China, Journal of Geophysical Research Atmospheres, 119(4), 1903–1914, 2014.

Wang, Z. F., Ueda, H., & Huang, M. : A deflation module for use in modeling long-range transport of yellow sand over East Asia, Journal of Geophysical Research Atmospheres, 105(D22), 26947-26959, 2000.

Wang, Z., Li, J., Wang, X., Pochanart, P., & Akimoto, H. : Modeling of regional high ozone episode observed at two mountain sites (MT. Tai and Huang) in East China. Journal of Atmospheric Chemistry, 55(3), 253-272, 2006a.

Wang, Z. F., Xie, F. Y., Wang X. Q., An J. L., Zhu, J. : Development and Application of Nested Air Quality Prediction Modeling System, Chinese Journal of Atmospheric Sciences, 30(5),778-790, 2006b. (in Chinese)

Wang, Z. F., Xie, F., Sakurai, T., Ueda, H., Han, Z., & Carmichael, G. R., et al. : Mics-Asia II: model inter-comparison and evaluation of acid deposition, Atmospheric Environment, 42(15), 3528-3542, 2008.

Wang, Z. F., Pang, C. M., Zhu, J., et al. : IAP Progress in Atmospheric Environment Modeling Research, Chinese Journal of Atmospheric Sciences, (04): 987-995, 2008. (in Chinese)

Wei, Y., Li, J., Wang, Z. F., Chen, H. S., Wu, Q. Z., et al. : Trends of surface $PM_{2.5}$ over Beijing–Tianjin–Hebei in 2013–2015 and their causes: emission controls VS. meteorological conditions, Atmospheric and Oceanic Science Letters, 10(4), 276-283, 2017.

Wesely, M. L. : Parameterization of surface resistances to gaseous dry deposition in regional-scale numerical models, Atmospheric Environment, 23(6), 1293-1304, 1989.

Wu, J, Y. Xu, B. Zhang. : Projection of $PM_{2.5}$ and Ozone Concentration Changes over the Jing-Jin-Ji Region in China, Atmospheric and Oceanic Science Letters 8(3):143-146, 2015.

Wu, J. B., Wang, Z., Qian, W., Jie, L., Xu, J., & Chen, H. S., et al. : Development of an on-line source-tagged model for sulfate, nitrate and ammonium: a modeling study for highly polluted periods in Shanghai, China, Environmental Pollution, 221, 168-179, 2017.

Wu, Q. Z., Z. F. Wang, et al. : A numerical study of contributions to air pollution in Beijing during CAREBeijing-2006, Atmospheric Chemistry and Physics, 11(12), 5997-6011, 2011.

Wu, Q., Wang, Z., Chen, H., Zhou, W., & Wenig, M. : An evaluation of air quality modeling over the Pearl River Delta during November 2006, Meteorology & Atmospheric Physics, 116(3-4), 113-132, 2012.

Xiaoyuan Yan, Toshimasa Ohara, & Hajime Akimoto. : Statistical modeling of global soil NOx emissions. Global Biogeochemical Cycles, 19(3), 2005.

Zaveri, R. and L. Peters : A new lumped structure photochemical mechanism for large-scale application, Journal of Geophysical Research-Atmospheres, 104(D23), 1999.

Zhang, L. M., Brook, J. R., & Vet, R. : A revised parameterization for gaseous dry deposition in air-quality models, Atmos.chem.phys, 3(2), 2067-2082, 2003.

Zhang, Q., Quan, J., Tie, X., Li, X., Liu, Q., & Gao, Y., et al. : Effects of meteorology and secondary particle formation on visibility during heavy haze events in Beijing, China, Science of the Total Environment, 502, 578-584, 2015.

Zhang, X. Y., Wang, Y. Q., Zhang, X. C., Guo, W., & Gong, S. L. : Carbonaceous aerosol composition over various regions of china during 2006, Journal of Geophysical Research,

Atmospheric
Chemistry
and Physics
Discussions

113(D14), 2008.

Zhang, Y., Karamchandani, P., Glotfelty, T., Streets, D. G., Grell, G., & Nenes, A., et al. : Development and initial application of the global-through-urban weather research and forecasting model with chemistry (GU-WRF/Chem), Journal of Geophysical Research Atmospheres, 117(D20), 2012.

950

Zeng, Q. C., Zhou, G. Q., Pu, Y. F., Chen, W., Li, R. F., Liao, H., et al. : Research on the Earth System Dynamic Model and Some Related Numerical Simulations. Chinese Journal of Atmospheric Sciences, 32(4), 653-690, 2008. (in Chinese)

Zheng, B., Zhang, Q., Zhang, Y., He, K. B., Wang, K., & Zheng, G. J., et al. : Heterogeneous

955

chemistry: a mechanism missing in current models to explain secondary inorganic aerosol formation during the January 2013 haze episode in North China, Atmospheric Chemistry & Physics, 14(15), 2031-2049, 2015.

Zheng, B., Tong, D., Li, M., Liu, F., Hong, C. P., Geng, G. N., et al. : Trends in China's anthropogenic emissions since 2010 as the consequence of clean air actions, Atmospheric

960

Chemistry & Physics Discussions, 13(5), 2607-2634. doi:10.5194/acp-15-2031-2015, 2018.

Zhu, J., Zeng, X., Zhang, M., Dai, Y., Ji, D., & Li, F., et al. : Evaluation of the new dynamic global vegetation model in CAS-ESM, Advances in Atmospheric Sciences, 35(6), 659-670, 2018.

39

Atmospheric
Chemistry
and Physics
Discussions

Figures
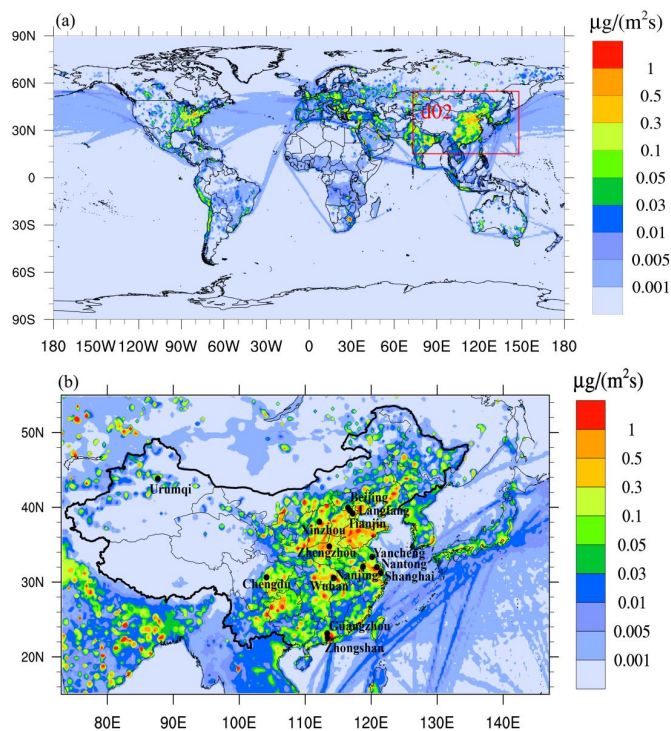
965

Fig. 1. The simulation domain with total SO_2 emission ($\mu g\ m^{-2}\ s^{-1}$). (a) domain 1; (b) domain 2, black circles are locations of the city sites in China.

Atmospheric
Chemistry
and Physics
Discussions

Open Access

EGU
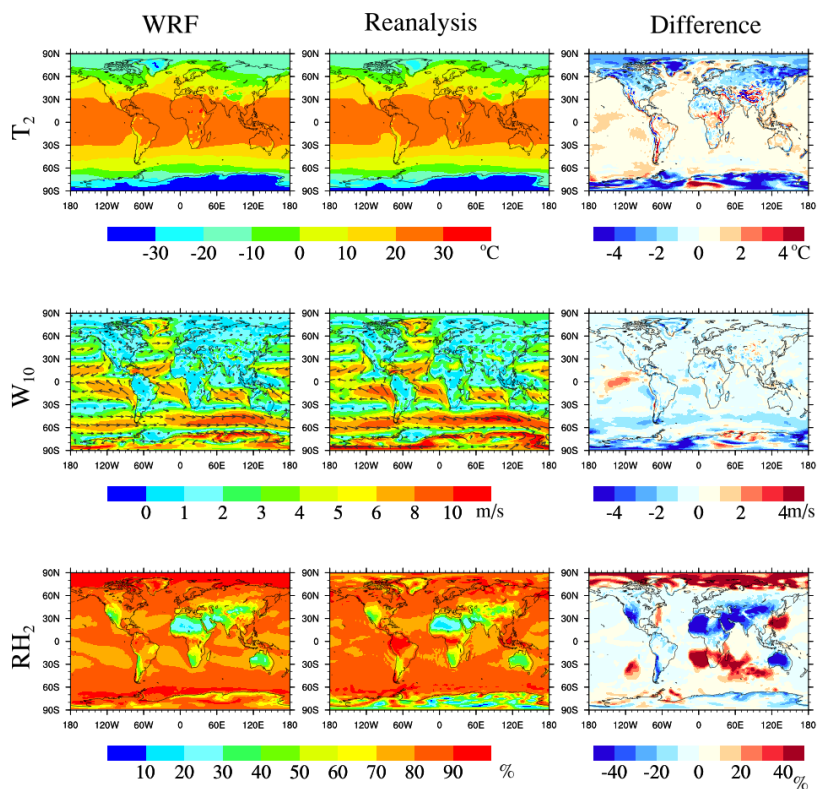
Fig. 2. Comparison of annual meteorological fields. The left column is WRF simulation, the middle column is reanalysis data, and the right column is the difference between simulation and reanalysis (WRF-Reanalysis). The reanalysis data is NCEP Reanalysis1.
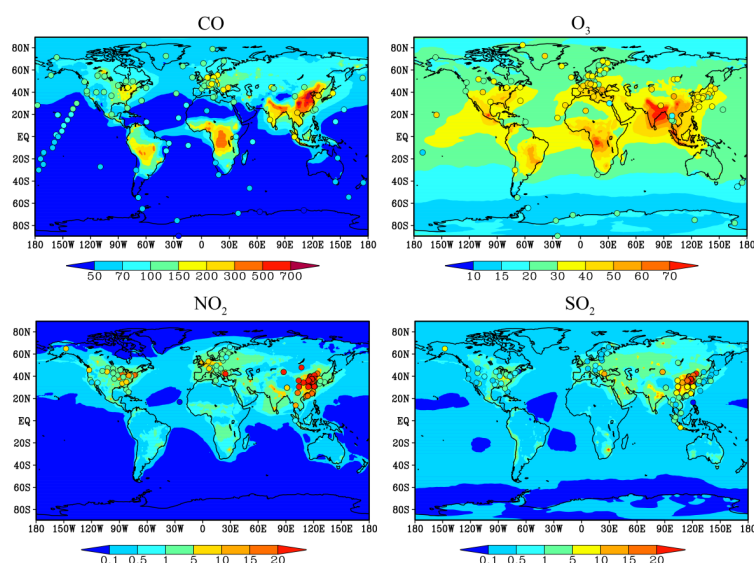
Fig. 3. Annual mean concentration (ppb) of the surface layer in IAP-AACM. The circles represent site observations. The first row is CO and O_3, the bottom row is NO_2 and SO_2.
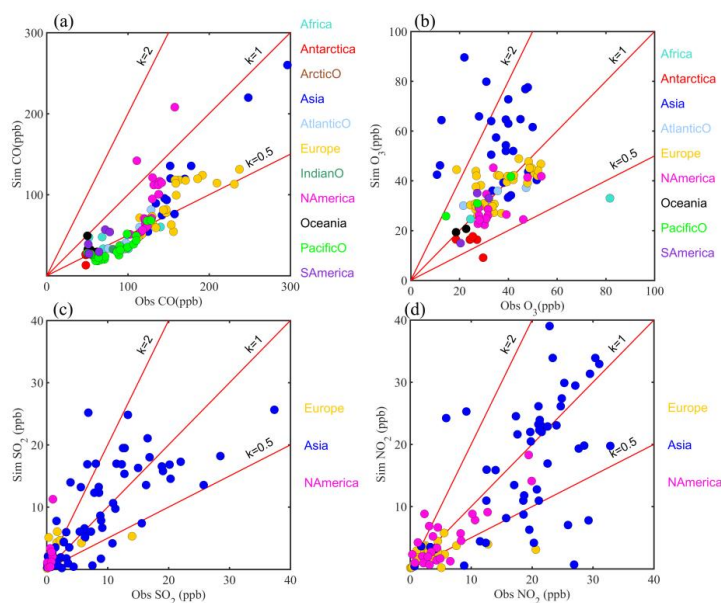
Fig. 4. Scatter plots of annual mean concentrations (ppb) in Africa, Antarctica, Arctic Ocean (ArcticO), Asia, Atlantic Ocean (AtlanticO), Europe, Indian Ocean (IndianO), North America (NAmerica), South America (SAmerica), Oceania and Pacific Ocean (PacificO). The abscissa shows the observation and the ordinate shows the simulation.

The color of the points represents different regions. (a) ~ (d) show CO, O_3, SO_2 and NO_2 respectively.

Atmospheric
Chemistry
and Physics
Discussions

Open Access

EGU
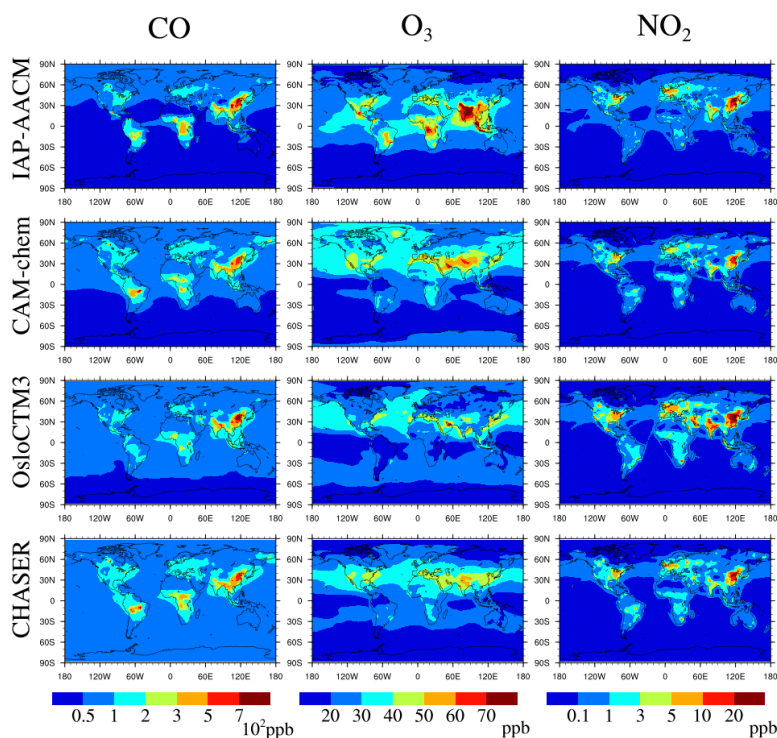
985

Fig. 5. Annual mean surface distributions (ppb) from IAP-AACM compared with HTAP models. Rows from top to bottom represent IAP-AACM, CAM-Chem, OsloCTM3 and CHASER respectively. The left column displays CO, the middle column displays O_3 and the right column is NO_2.
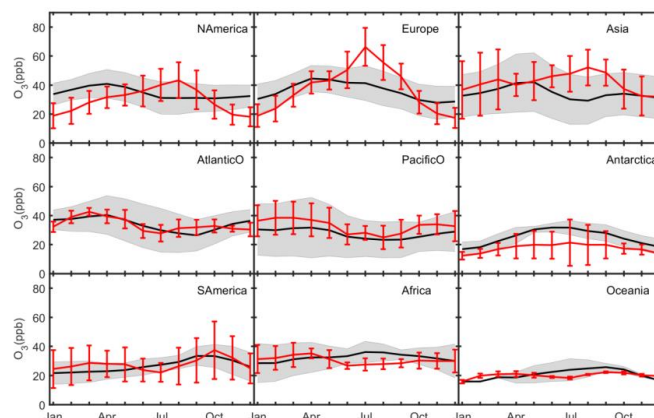
990

Fig. 6. Mean seasonal variation of O_3 (ppb) over NAmerica, Europe, Asia, AtlanticO, PacificO, Antarctica, SAmerica, Africa and Oceania sites. Black lines and red lines represent the average of observations and simulations respectively. Gray shaded areas and red vertical bars show 1 standard deviation over the sites for observations and for

995   model results respectively.

Fig. 7. The same as Fig. 3, except the species are sulfate, nitrate, ammonium, BC, OC, and PM$_{2.5}$ and the unit is μg m^{-3}.
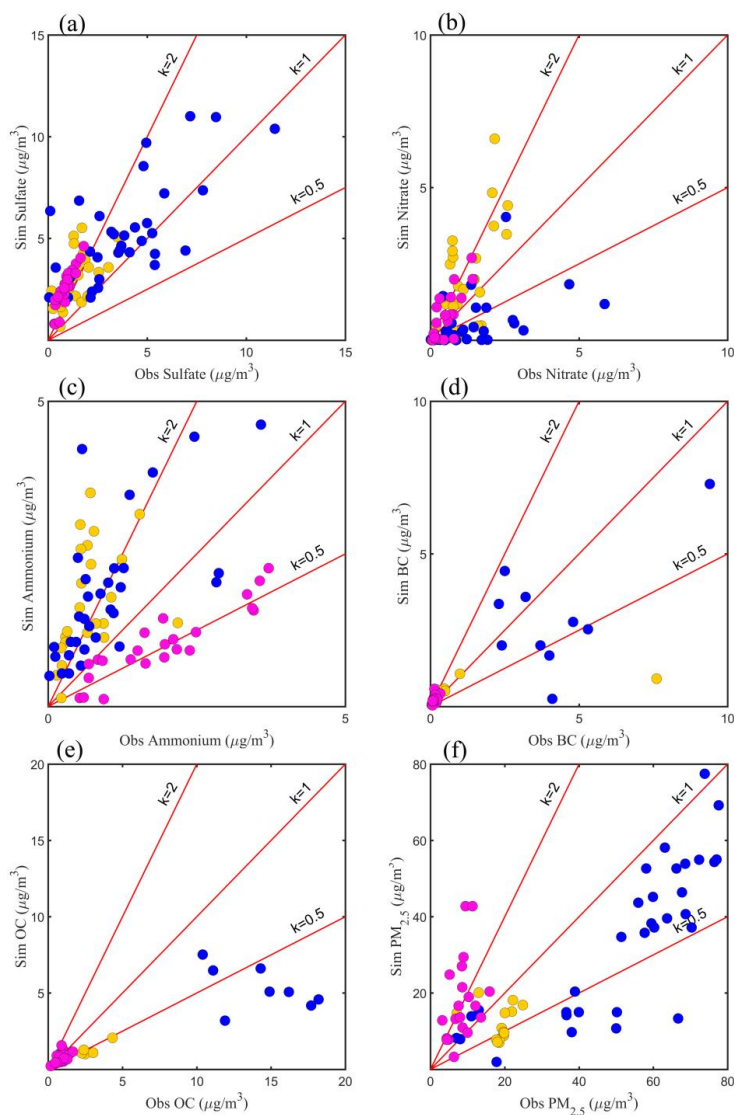
1000

Fig. 8. Scatter plot of annual mean concentration (µg m^{-3}) in Europe, Asia and NAmerica. (a)~(f) is sulfate, nitrate, ammonium, BC, OC and PM$_{2.5}$ respectively. The abscissa shows the observation and the ordinate shows the simulation. The regions represented by different colors are consistent with Fig. 4c
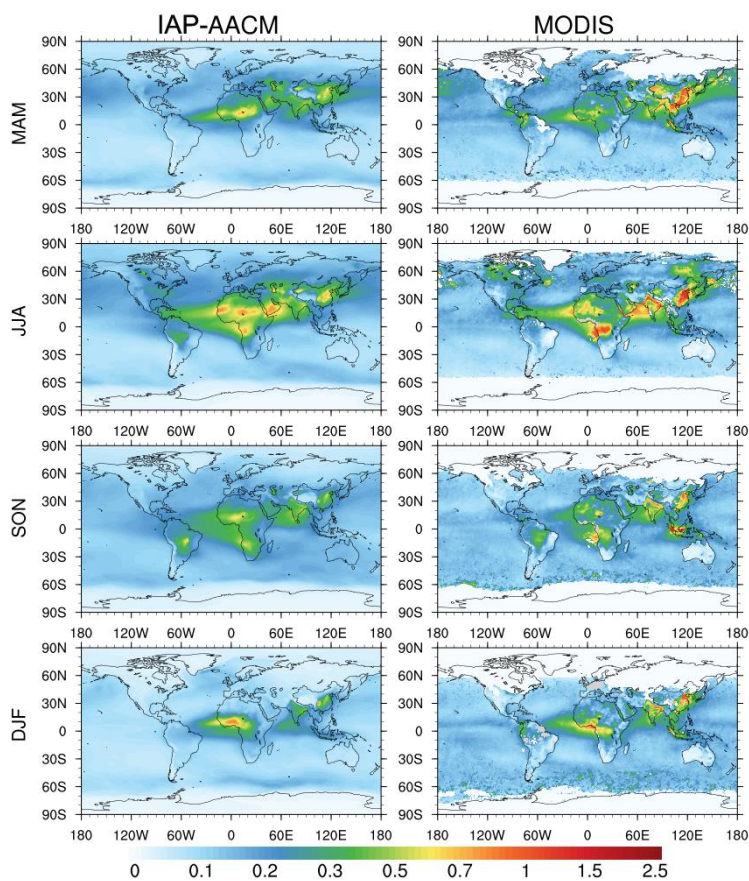
1005

Fig. 9. Seasonal mean AOD from IAP-AACM and MODIS. Seasons are defined as December-January-February (DJF), March-April-May (MAM), June-July-August (JJA), and September-October-November (SON).
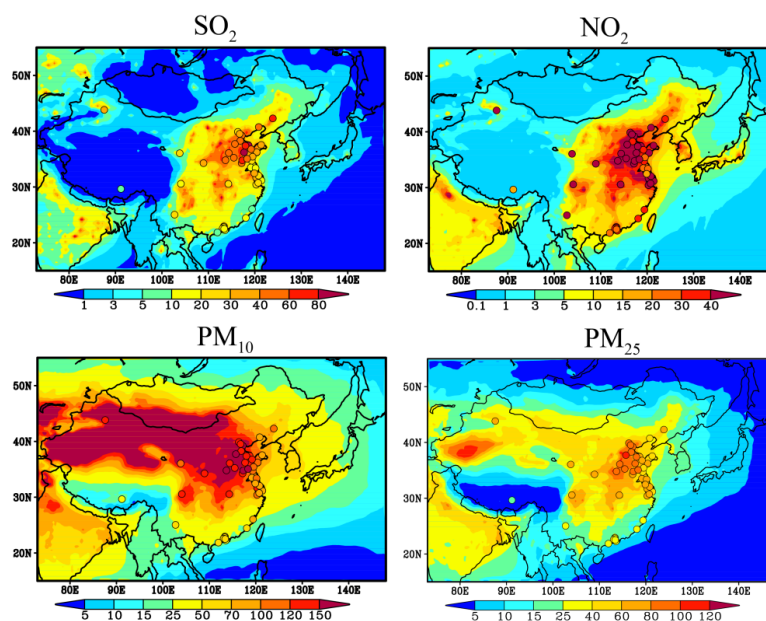
1010   Fig. 10. Surface annual mean concentration (μg m^{-3}) of the nested domain. The circles represent sites observations. The top row is SO$_2$ and NO$_2$, the bottom row is PM$_{10}$ and PM$_{2.5}$.

Atmospheric
Chemistry
and Physics
Discussions
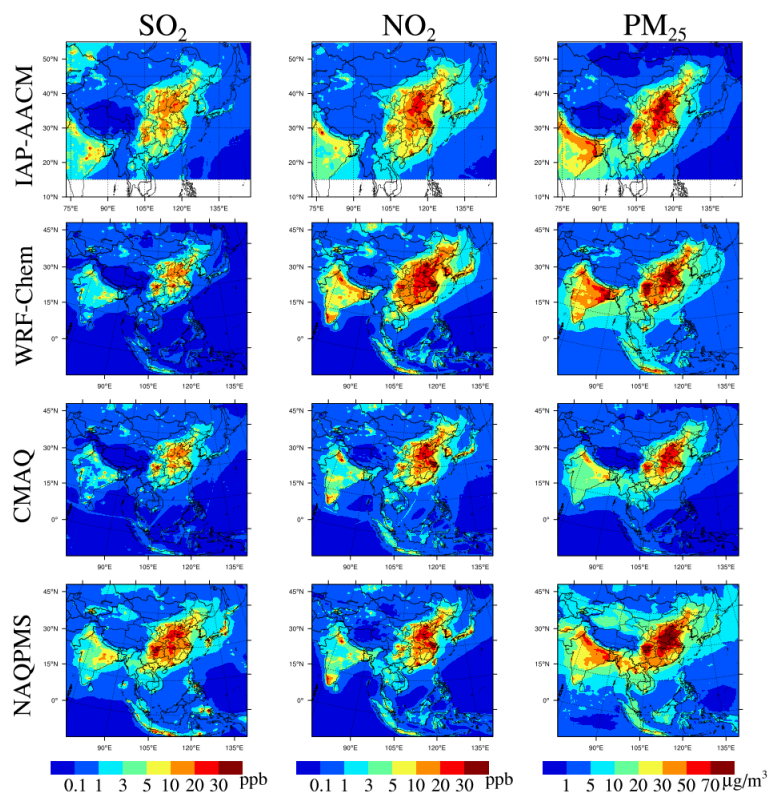
1015   Fig. 11. Annual surface distributions from nested IAP-AACM compared with regional models from MICS-Asia. Each row from top to bottom represents IAP-AACM, WRF-Chem, CMAQ and NAQPMS respectively. The left column is SO$_2$, the middle column is NO$_2$ and the right column is PM$_{2.5}$. The unit for gases is ppb and for particles is μg m^{-3}.
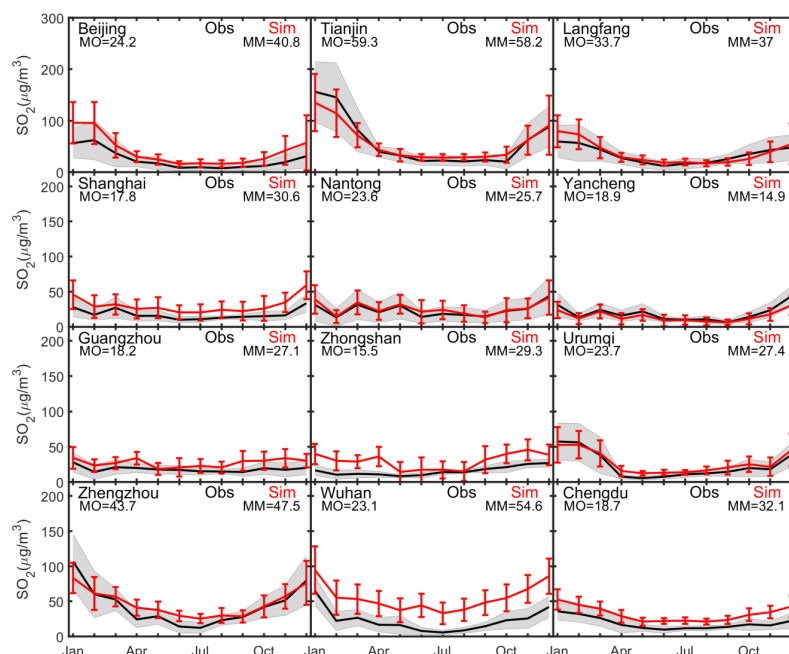
1020

Fig. 12. Mean seasonal variation of SO_2 (μg m^{-3}) over China. The black line and red line represent monthly mean concentration of city-averaged observation and simulation respectively. Gray shaded areas and red vertical bars show 1 standard deviation over the sites for observations and for model results, respectively. MO and MM stand for annual mean concentration of observation and simulation respectively.
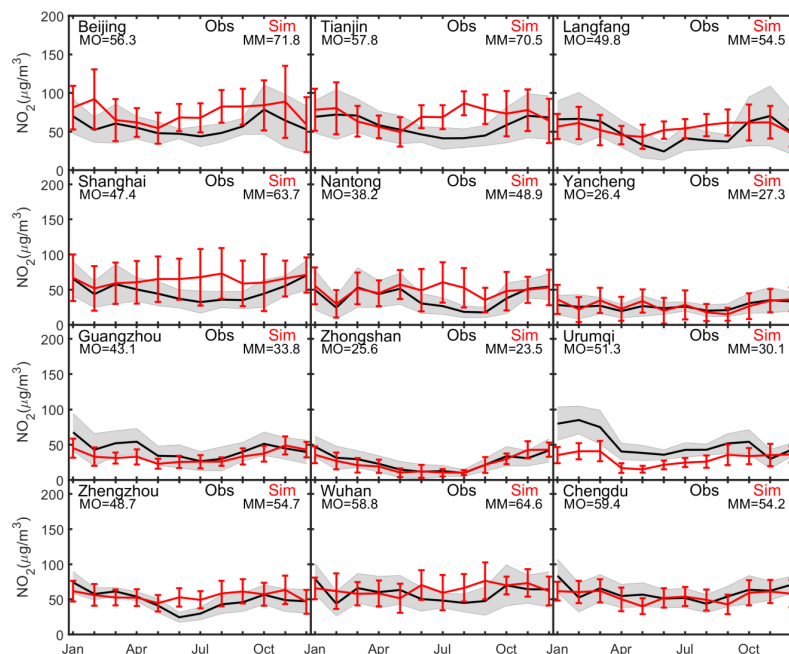
1025
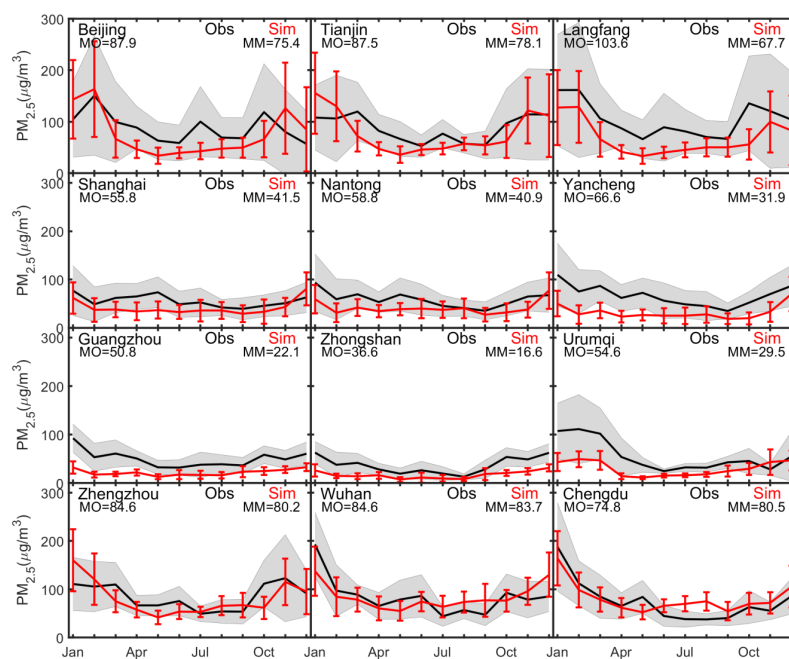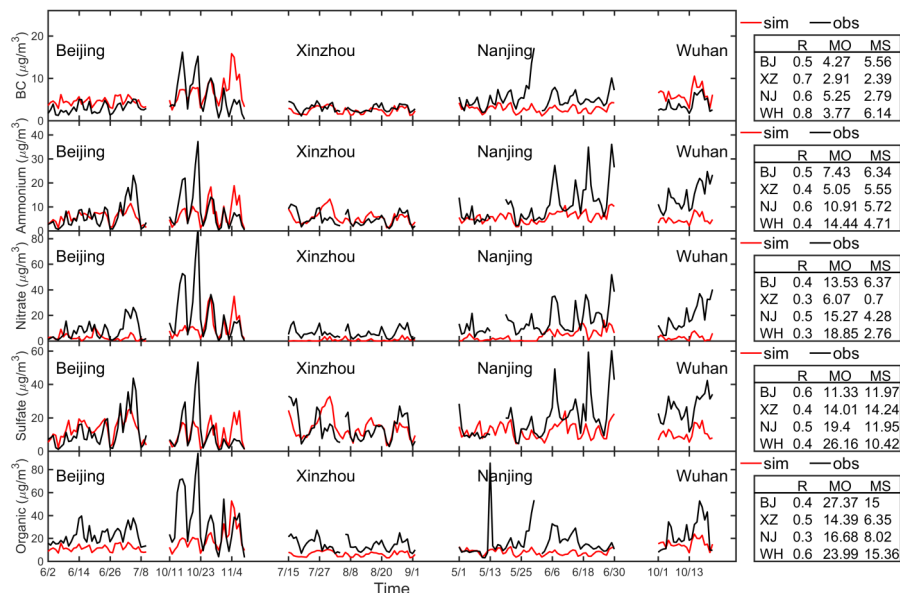
Fig. 13. The same as Fig. 12, except the pollutant is NO_2.

Fig. 14. The same as Fig. 12, except the pollutant is $PM_{2.5}$.

Atmospheric
Chemistry
and Physics
Discussions

Fig. 15. Daily variation of aerosol components (µg m^{-3}) over China. The black line and red line represent daily mean concentration of city-averaged observation and simulation respectively. BJ, XZ, NJ and WH mean Beijing, Xinzhou, Nanjing and Wuhan respectively. R, MO and MM stand for correlation coefficient, mean concentration of observation and model respectively.

Atmospheric
Chemistry
and Physics
Discussions

Tables

Table 1. Emissions used in IAP-AACM

Database	Abbreviation	Base year	Source type	Reference
Hemispheric Transport of Air Pollution version2	HTAP-v2	2010	Anthropogenic	Janssens-maenhout et al., 2015
Global Fire Emissions Database version4	GFED-v4	2010	Biomass burning	Randerson et al., 2015
Model of Emissions of Gases and Aerosols from Nature–Monitoring Atmospheric Composition and Climate	MEGAN-MACC	2010	Biogenic	Sindelarova et al., 2014
Regional Emission inventory in Asia	REAS	2001	Soil (NOx)	Yan et al., 2005
Precursors of Ozone and their Effects in the Troposphere	POET	2000	Ocean (VOCs)	Granier et al., 2005
Global Emission InitiAtive	GEIA	Average of 1983 ~ 1990	Lightning (NOx)	Price et al., 1997

1040

Table 2. Summary of statistical of annual and seasonal meteorology in the nested domain compared with NCDC sites. Seasons are defined as spring (March–May), summer (June–August), fall (September–November), and winter (December–February).

	Period	MO	MM	RMSE	R
T_2	2014	17.6	17.5	1.8	0.98
	Spring	16.3	16.2	1.9	0.97
	Summer	24.3	24.0	2.0	0.93
	Autumn	17.2	17.0	1.7	0.97
	Winter	9.5	9.5	1.7	0.96
W_{10}	2014	3.1	2.5	1.5	0.53
	Spring	3.2	2.7	1.8	0.61
	Summer	2.9	2.1	1.9	0.48
	Autumn	3.0	2.3	1.7	0.53
	Winter	3.1	2.4	1.8	0.56
RH_2	2014	64.8	61.7	12.3	0.84
	Spring	58.5	56.2	12.6	0.86
	Summer	71.2	68.0	11.7	0.86
	Autumn	68.1	64.0	11.7	0.83
	Winter	61.4	58.6	13.2	0.76

1045

Atmospheric
Chemistry
and Physics
Discussions

Table 3. Summary of the site observation datasets

Dataset	Site number	Year	Observed species
WDCGG	169	Average of 2006~2015	CO, O_3, SO_2, NO_2
EANET	41	2014	SO_2, NO_2, O_3, $PM_{2.5}$, sulfate, nitrate, ammonium
EMEP	46	2014	$PM_{2.5}$, BC, OC, sulfate, nitrate, ammonium
IMPROVE	23	2014	$PM_{2.5}$, BC, OC, sulfate, nitrate, ammonium
EPA	93	2014	SO_2, NO_2, $PM_{2.5}$
CAWNET	13	2006	BC, OC
CNEMC	89	2014	CO, O_3, SO_2, NO_2, PM_{10}, $PM_{2.5}$
Others	4	2014	BC, OM, sulfate, nitrate, ammonium

Table 4. Global budgets for DMS, SO_2 and sulfate

Species		IAP-AACM	Other models[a]
DMS	Sources (Tg S yr^{-1})	22.8	
	Emission	22.8	10.7~23.7
	Sinks (Tg S yr^{-1})	22.8	
	Dry deposition	0.0	
	Oxidation	22.8	
	Burden (Tg S)	0.19 ↑[b]	0.02~0.15
	Lifetime (days)	3	0.5~3.0
SO_2	Sources (Tg S yr^{-1})	77.1	
	Emission	54.3 ↓[b]	63.4~94.9
	DMS oxidation	22.8	10.0~25.6
	Sinks (Tg S yr^{-1})	77.1	
	Dry deposition	28.0	16.0~55.0
	Wet deposition	0.0	0~19.9
	Gas-phase oxidation	19.3	6.1~22.0
	Aqueous-phase oxidation	29.8	24.5~57.8
	Burden (Tg S)	0.63	0.2~0.69
	Lifetime (days)	3.0 ↑[b]	0.6~2.6
Sulfate	Sources (Tg S yr^{-1})	50.5	
	Emission	1.4	0~3.5
	Gas-phase oxidation	19.3	6.1~22.0
	Aqueous-phase oxidation	29.8	24.5~57.8
	Sinks (Tg S yr^{-1})	50.5	
	Dry deposition	2.9	0.8~18.0
	Wet deposition	47.6	34.7~61.1
	Burden (Tg S)	0.82	0.38~1.07
	Lifetime (days)	5.9	3.0~7.9

[a] including Liu et al. (2005), Lee et al. (2015), and those listed in Liu et al. (2005), the range
of sulfate is also refer to the GISS-TOMAS (Lee et al., 2010), ACCMIP (Lee et al., 2013) and the
AeroCom (Textor et al., 2006) results.

[b] outside the range of other models

Table 5. Global budgets for carbonaceous aerosol

Species		IAP-AACM	Other models[a]
	Sources (Tg yr^{-1})	7.42	
	Emission	7.42	7.4~19.0
	Sinks (Tg yr^{-1})	7.42	
BC	Dry deposition	1.01	0.3~4.6
	Wet deposition	6.41	3.8~13.7
	Burden (Tg)	0.13	0.08~0.59
	Lifetime (days)	6.4	3.3~9.4
	Sources (Tg yr^{-1})	56.7	50~216
	Emission	48.7	34~144
	Sinks (Tg yr^{-1})		
OM[b]	Dry deposition	6.79	2~36
	Wet deposition	49.9	28~209
	Burden (Tg)	1.16	0.7~3.8
	Lifetime (days)	7.4	3.5~9.2

[a] including Liu et al. (2005), Lee et al. (2010), Lee et al. (2013), Lee et al. (2015), Textor et al.
(2006), and those listed in Liu et al. (2005).

[b] the convert factor from OC to OM is 1.7 in IAP-AACM.

Table 6. The NMB of annual average concentration in different regions. ASO$_4$, ANO$_3$
and ANH$_4$ represents sulfate, nitrate and ammonium, respectively.

	CO	O$_3$	SO$_2$	NO$_2$	ASO$_4$	ANO$_3$	ANH$_4$	BC	OC	PM$_{2.5}$
Africa	-0.48	-0.37								
Antarctica	-0.5	-0.31								
ArcticO	-0.45									
Asia	-0.28	0.86	0.25	-0.59	0.36	-0.61	0.85	-0.4	-0.67	-0.36
AtlanticO	-0.48	0.01								
Europe	-0.43	0.03	0.52	-0.39	1.1	0.74	1.49	-0.62	-0.55	-0.35
IndianO	-0.54									
NAmerica	-0.26	-0.14	3.52	-0.14	1.94	0.50	-0.46	0.64	-0.12	1.16
Oceania	-0.34	-0.03								
PacificO	-0.59	0.13								
SAmerica	-0.36	0.05								

Atmospheric
Chemistry
and Physics
Discussions

Table 7. Summary of statistics for global and nested domains. D1 and D2 represents results of domain 1 and domain 2, respectively.

Species	City	R		RMSE (µg m⁻³)		MB (µg m⁻³)		NMB	
		D1	D2	D1	D2	D1	D2	D1	D2
PM$_{2.5}$	Beijing	0.69	0.70	54.28	55.65	-12.33	-16.89	-0.14	-0.19
	Tianjin	0.67	0.72	46.63	46.51	-11.00	-13.27	-0.13	-0.15
	Langfang	0.72	0.79	66.02	65.22	-28.58	-38.34	-0.28	-0.37
	Shanghai	0.71	0.71	29.51	27.99	-18.23	-16.00	-0.33	-0.29
	Nantong	0.69	0.75	31.46	29.70	-18.32	-17.84	-0.31	-0.30
	Yancheng	0.74	0.80	45.52	43.30	-35.60	-33.99	-0.53	-0.51
	Guangzhou	0.43	0.63	38.75	36.91	-29.91	-29.39	-0.59	-0.58
	Zhongshan	0.51	0.76	26.16	26.77	-16.08	-20.38	-0.44	-0.56
	Urumqi	0.31	0.50	59.32	48.10	-38.40	-25.88	-0.70	-0.47
	Zhengzhou	0.59	0.63	41.98	43.05	0.70	-7.30	0.01	-0.09
	Wuhan	0.57	0.64	44.49	42.28	-11.32	-12.09	-0.13	-0.14
	Chengdu	0.76	0.77	37.18	36.14	5.23	-0.19	0.07	0.00
SO$_2$	Beijing	0.87	0.89	26.99	25.00	21.32	16.58	0.88	0.68
	Tianjin	0.85	0.85	35.45	29.51	-10.96	-1.10	-0.18	-0.02
	Langfang	0.74	0.76	24.65	18.90	11.49	3.38	0.34	0.10
	Shanghai	0.50	0.75	38.48	18.10	30.43	12.76	1.71	0.72
	Nantong	0.69	0.78	13.55	12.08	-0.23	2.17	-0.01	0.09
	Yancheng	0.78	0.83	9.75	8.79	-4.29	-4.02	-0.23	-0.21
	Guangzhou	0.26	0.40	10.42	14.96	-0.96	8.86	-0.05	0.49
	Zhongshan	0.59	0.33	7.33	21.65	1.65	13.74	0.11	0.88
	Urumqi	0.63	0.60	23.04	20.01	-11.88	3.68	-0.50	0.16
	Zhengzhou	0.79	0.82	24.51	20.06	12.34	3.84	0.28	0.09
	Wuhan	0.70	0.48	18.72	40.28	12.03	31.47	0.52	1.36
	Chengdu	0.52	0.60	48.52	17.61	44.44	13.33	2.37	0.71
NO$_2$	Beijing	0.48	0.68	26.00	26.82	11.98	15.68	0.21	0.28
	Tianjin	0.41	0.51	26.24	27.39	9.88	13.02	0.17	0.23
	Langfang	0.39	0.53	33.84	23.83	19.60	4.91	0.39	0.10
	Shanghai	0.57	0.56	29.28	32.17	8.79	16.79	0.19	0.35
	Nantong	0.60	0.59	21.86	24.11	3.63	10.69	0.10	0.28
	Yancheng	0.44	0.49	18.33	16.53	-1.55	1.78	-0.06	0.07
	Guangzhou	0.40	0.51	28.34	20.28	-20.41	-9.19	-0.47	-0.21
	Zhongshan	0.63	0.70	13.47	12.51	-3.01	-2.06	-0.12	-0.08
	Urumqi	0.24	0.41	41.73	30.31	-35.18	-21.39	-0.69	-0.42
	Zhengzhou	0.32	0.44	23.68	18.75	13.65	5.97	0.28	0.12
	Wuhan	0.25	0.22	25.36	28.39	5.77	6.16	0.10	0.10
	Chengdu	0.31	0.43	27.26	20.77	-18.88	-5.84	-0.32	-0.10

1065